Water Vapor Transport and its Influence on Water Stable Isotope in Dongting Lake Basin

Xiong Xiao[1], Xinping Zhang[1,2]*, Zhuoyong Xiao[1], Zhongli Liu[1], Dizhou Wang[1],

Cicheng Zhang[1], Zhiguo Rao[1], Xinguang He[1,2], Huade Guan[3]

[1] *College of Geographic Science, Hunan Normal University, Changsha 410081, China*

[2] *Key Laboratory of Geospatial Big Data Mining and Applications in Hunan Province,*

Hunan Normal University, Changsha 410081, China

[3] *College of Science and Engineering, Flinders University, Adelaide SA 5001, Australia*

ABSTRACT: Understanding water vapor sources and transport paths is essential for assessing the water cycle and predicting precipitation accurately. Utilizing water vapor diagnosis and calculations, this study determined the water vapor sources and transport paths leading to precipitation in the Dongting Lake Basin in four seasons (represented by January, April, June, and October). In January, the water vapor generating precipitation originated from the Arabian Peninsula, driven by the southern branch of the westerlies over the southern side of the Tibetan Plateau, along the northern side of the Indian Peninsula through southwest China to reach the Dongting Lake Basin. In April, two transport paths emerged: one aligned closely with the January transport path but the location shifted slightly northward by one degree of latitude, and another was driven by the weak subtropical high over the southwestern Pacific, bringing moist air from the western Pacific via the South China Sea and Indochinese Peninsula. In June, the vapor sourced from the northern branch of the South Indian Ocean subtropical high

---

* Corresponding author. Tel.: +86-13308486020; E-mail address: zxp@hunnu.edu.cn

crossed the equator and transported through various water bodies to southwestern China,

finally reaching the basin. October saw a water vapor transport path from the western

Pacific, crossing the South China Sea, and entering the Dongting Lake Basin influenced

by the East Asian monsoon system. In different seasons, the variations in water stable

isotopes along water vapor transport paths show some agreement with Rayleigh

fractionation and water balance principles, as reflected in the model simulations and

observations~~In different seasons, the variations in water stable isotopes along water~~

~~vapor transport paths adhered to Rayleigh fractionation and water balance principles~~.

These findings highlight the impact of atmospheric circulation on precipitation and

isotopes, providing a framework for understanding water vapor isotope mechanisms

and reconstructing past atmospheric conditions.

Keywords: Dongting Lake Basin; Water vapor sources; Transport paths; Precipitation

isotopes; Precipitation amount.

Significance Statement

This research explored how water vapor transports influenced the precipitation isotopes

in the Dongting Lake Basin in representative months of different seasons. By tracking

water vapor from its source regions, we revealed the influence of large-scale

atmospheric circulation on the transportation of water vapor to the Dongting Lake Basin.

The changes in water stable isotopes along the water vapor transport paths highlighted

the isotopic fractionation and water vapor exchange that occurred along these paths,

while the isotopic changes in the precipitation reflect the cumulative influences of water

vapor transport on the local precipitation. These comprehensive insights have clarified

the influences of atmospheric circulation on water vapor transport and precipitation

isotopes, and are thus essential for predicting regional precipitation patterns.

1. Introduction

Diagnosing water vapor sources and analyzing water vapor transport are routine

and foundational tasks, particularly within hydrometeorological services (Gimeno et al.,

2020; Xu et al., 2020). A correct understanding of water vapor sources and transport is

crucial for accurately evaluating the hydrological cycle and effectively predicting

precipitation. For instance, in weather forecasting for the East Asian region, an essential

condition for the occurrence of precipitation is the presence of sufficiently warm and

moist air from low latitudes (Barker, et al., 2015; Tang et al., 2015; Hu et al., 2021).

Moreover, the primary cause of meteorological drought in the East Asian monsoon

region is often attributed to an anomalous decrease in water vapor sourced from the

Bay of Bengal (He et al., 2022; Liu et al., 2023).

Over the past few decades, the employment of diverse mathematical models has

been the crucial approach to tracking and deducing atmospheric water vapor sources

and transport paths (Gimeno et al., 2020; Xu et al., 2020; Pranindita et al., 2022;

Lekshmy et al., 2022). For instance, Pranindita et al. (2022) employed the water vapor

tracking model WAM-2layers to trace back the water vapor sources during heatwaves

in northern, western, and southern Europe, the reasons for the reduction of the local

precipitation can be attributed to a significant reduction in water vapor supply from the

North Atlantic due to anticyclonic patterns, along with the increased water vapor fluxes

from eastern Eurasia and local regions. Utilizing the Lagrangian model FLEXPART

v9.0, Pérez-Alarcón et al. (2023) identified precipitation water vapor sources associated

with the development of Indian Ocean tropical cyclones. Results showed that the water

vapor sources and transport mechanisms were different during different lifecycle stages

of tropical cyclones. Among numerous methods, the use of HYSPLIT for tracking water

vapor sources is widespread, which employs backward trajectory calculations and

atmospheric wind field information to derive water vapor transport trajectories at given

heights during a precipitation event, making it commonly used for tracing water vapor

during short-duration precipitation events (Draxler and Hess, 1998; Esquivel-

Hernández et al., 2019; Nie and Sun, 2022). However, due to inherent model structure

and tracking principles, derived water vapor transport paths at different heights may

vary or even be opposite. Moreover, this method cannot ascertain whether the tracked

water vapor indeed causes precipitation, nor can it provide information on the

magnitude of water vapor transport (Wu et al., 2015; Wu et al., 2022; Deng et al., 2024).

With the continuous improvement of observational techniques and analytical

methods, utilizing reanalysis data to determine the water vapor sources that cause

precipitation has become a common practice (Sun et al., 2011; Hoffmann et al., 2019;

Guo et al., 2019; Shi et al., 2022). For instance, Sun et al. (2011) investigated the

climatic characteristics and decadal variations in water vapor transport in Eastern China

based on NCEP/NCAR reanalysis data from 1979 to 2009. The results revealed that the

variability in water vapor transport in the region is attributed to the combined influences

of the Indian summer monsoon and the East Asian summer monsoon. Zhou et al. (2018)

analyzed the correlation between precipitation $\delta^{18}O$ and water vapor transport during

the warm half-year (April to September) in China using GNIP data and NCEP/NCAR reanalysis datasets. Their study found a significant negative correlation between precipitation $\delta^{18}O$ and water vapor transport from the southwest direction, indicating that the southwest monsoon, which brings water vapor from the Indian Ocean, plays a crucial role in precipitation formation. In contrast, the relationship between precipitation and water vapor transport from the northwest direction is not significant and even shows an inverse relationship in some cases. This suggests that water vapor transport from the northwest has a minimal direct influence on precipitation in the Changsha region. Since the direction of water vapor transport has an important influence on regional precipitation, it is necessary to reveal the influences of atmospheric circulation such as the water vapor source regions and water vapor transport paths, which determine the water vapor transport direction.

Water vapor transport controlled by atmospheric circulation not only determines precipitation events but also directly influences the precipitation isotopes, thus analyzing the water vapor sources and water vapor transport paths, as well as their influences on stable isotopes under different seasons, can elucidate the mechanisms influencing the atmospheric stable isotopes (Zhou et al., 2019; Dahinden et al., 2021; Zhan et al., 2023). For instance, Risi et al. (2010) conducted an analysis of water vapor and precipitation isotopes in the Sahelian region by combining water vapor budget and water vapor transport calculations, revealing that the isotopic composition of precipitation and atmospheric water vapor in the region is controlled by the intensity of air dehydration and changes in convection. Similarly, Sengupta et al. (2006) quantified

the influences of different water vapor source regions on precipitation in the northern

Indian monsoon region, finding that the isotopic composition of precipitation in the

region is influenced by changes in water vapor source and atmospheric circulations over

India. Moreover, Zhou et al. (2019) separately computed the correlations between $\delta^{18}O$

values of precipitation at different sites and found that during the prevalence of the

summer monsoon (April to September) and winter monsoon (October to March), the

key upstream regions influencing the precipitation isotopes in the Dongting Lake Basin

located in south-central China were the Bay of Bengal and southwestern China,

respectively. However, as the critical regions influencing regional precipitation isotopes

may not necessarily be the water vapor source regions, these studies are yet to

definitively determine the water vapor source regions and water vapor transport paths.

Assessing whether the stable isotopic composition of water vapor shows changes

consistent with Rayleigh distillation during transport, and evaluating the impact of this

transport on the isotopic composition of regional precipitation, are important research

objectives~~Verifying whether the stable isotopic composition of water vapor undergoes~~

~~changes consistent with Rayleigh distillation during transport, and assessing the impact~~

~~of this transport on the isotopic composition of regional precipitation, constitute~~

~~significant research objectives~~. Existing studies indicate that in the East Asian monsoon

region, including the Dongting Lake Basin, differences in the water vapor sources and

transport direction during different seasons are the primary drivers of seasonal

variations in precipitation isotopes (Araguás-Araguás et al., 1998; Zhang et al., 2016;

Wei et al., 2018; Chiang et al., 2020). Typically, during the summer monsoon,

132   prevailing southeast or southwest winds dominate the East Asian monsoon region, with

133   water vapor for precipitation originating from low-latitude oceans (Barker, et al., 2015;

134   Wu et al., 2015; Tang et al., 2015), while precipitation isotopes are significantly

135   depleted influenced by intense rainout effects along the water vapor transport paths

136   during this period (Zhou et al., 2019; Wu et al., 2022). Conversely, during the winter

137   monsoon, northwest or northeast winds prevail in the East Asian monsoon region, the

138   precipitation isotopes should be more enriched if water vapor for precipitation is carried

139   by westerlies or originates from the evaporation of inland regions (e.g., Liu et al., 2011;

140   Wu et al., 2015; Shi et al., 2021). However, both actual observations from the Global

141   Network of Isotopes in Precipitation (GNIP) and simulations from isotope-enabled

142   General Circulation Models (isoGCMs) consistently demonstrate that, whether during

143   the summer or winter monsoon, the spatial distribution of precipitation isotopes in the

144   East Asian monsoon region exhibits significant latitudinal and continental effects—that

145   is, the precipitation isotopes become more depleted with the increases of latitude or

146   distance from the ocean (Feng et al., 2009; Zhang et al., 2012; Zhang et al., 2016).

147   Consequently, the observed water vapor transport during the summer monsoon aligns

148   with the spatial distribution of precipitation isotopes under the influence of latitudinal

149   and continental effects and is consistent with the Rayleigh distillation principle for

150   water stable isotopes, however, water vapor transport during the winter monsoon does

151   not follow the above spatial distribution and Rayleigh distillation principle (Tang et al.,

152   2015; Zhou et al., 2019; Wu et al., 2022).

153   Based on the understanding outlined above, a thorough investigation into the

seasonal variations in water vapor sources and transport paths for precipitation amount

and isotopes in the East Asian monsoon region is necessary, which may provide

significant benefit for accurately understanding regional hydrological mechanisms and

elucidating regional climate characteristics. Focusing on the Dongting Lake Basin

within the East Asian monsoon area, and drawing upon fundamental theories of

meteorology, water vapor diagnostics, and water vapor calculations, a broader spatial

understanding of the scientific issues surrounding water vapor transport can be achieved.

This study aims to (1) identify the water vapor sources and transport paths contributing

to the Dongting Lake Basin; (2) analyze the variations in meteorological factors and

water stable isotopes along the water vapor transport paths; and (3) determine the

influences of different water vapor sources and transport paths on the regional

precipitation amounts~~reveal the mechanisms by which water vapor sources and~~

~~transport paths in the monsoon region influence precipitation amounts and isotopes~~.

2. Methods and materials

2.1 Study site

Dongting Lake Basin, situated in the south-central region of China (Fig. 1), is a

basin characterized by a subtropical monsoon climate, marked by distinct four seasons

and moderate humidity. Winters are wet and cold, while summers are warm and moist.

Based on historical meteorological data from 1960 to 2017, the Dongting Lake Basin

experiences an average annual precipitation of 1375.6.0 mm. During the colder months

(October to March of the following year), precipitation is relatively low due to the

influence of continental air masses. However, from late April onward, influenced by

oceanic monsoons, precipitation increases significantly, accompanied by a notable rise in temperature, with precipitation predominantly occurring from April to June (Liu et al., 2023; Xiao et al., 2024).
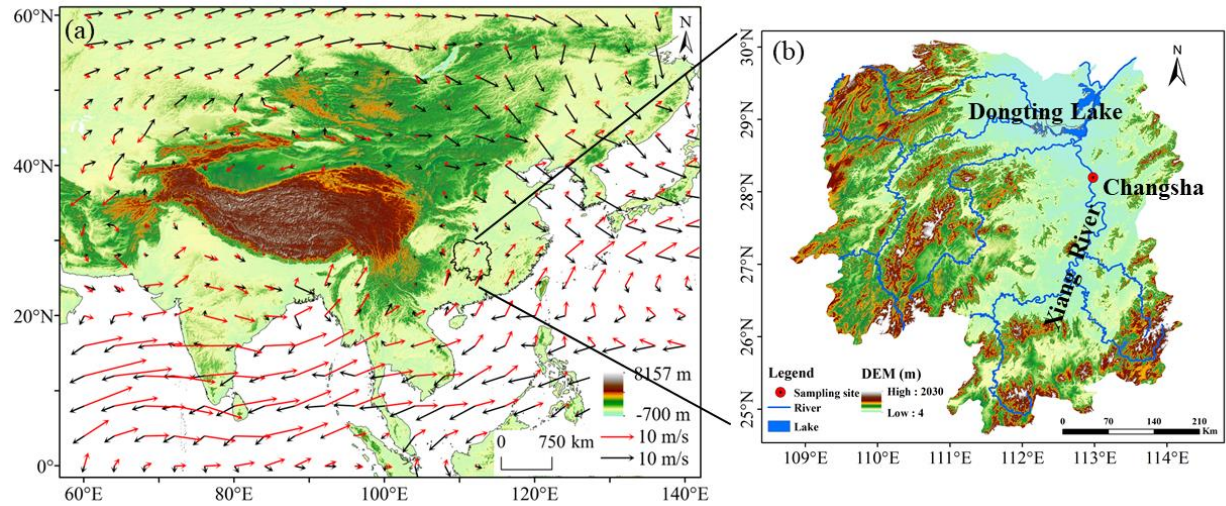
Fig. 1 Map showing the location of the Dongting Lake Basin, and the Changsha sampling site in the East Asian Monsoon Region. Note that the black arrow and red arrow in subplot (a) represent the average wind field at 850 hPa in January and June, respectively.

The prevailing wind refers to the wind or wind direction that appears the most frequently in a region during a specific period. Its occurrence is closely related to the changes in the average atmospheric circulation conditions due to the thermal differences between land and sea. In the East Asian monsoon region, which includes the Dongting Lake Basin, the strong cold high-pressure system influences the winter season, resulting in prevailing northerly winds at the lower troposphere, with northwesterly winds prevailing in the basin as shown by the average wind field at the 850 hPa in January, i.e. the black arrow in Fig. 1a. In the summer, influenced by the Western Pacific Subtropical High and the Indian Low, the winds at the lower

troposphere are predominantly southerly in the East Asian monsoon region, with southwesterly winds prevailing in the Dongting Lake Basin as shown by the average wind field at the 850 hPa in June, i.e. the red arrow in Fig. 1a. Positioned at the convergence of the prevailing northerly winds, prevailing southerly winds, and westerly winds, the Dongting Lake Basin experiences complex precipitation processes and different precipitation amounts in different seasons and water vapor transport directions. This complexity results in high variability in the precipitation isotope (Zhou et al., 2019; Xiao et al., 2024).

2.2 Water samples collection and measurement

From January 1, 2010 to December 31, 2022, precipitation sample sampling has been conducted at the Meteorological Garden of Hunan Normal University in Changsha (28°11'N, 112°56'E). The sampling protocol followed the meteorological observation standards of China's meteorological departments, with samples collected at 08:00 and 20:00 Beijing time on precipitation days. Liquid precipitation was directly collected in sealed 30 ml polyethylene bottles after measuring the precipitation amount, while solid precipitation was first collected in air-tight plastic bags, then measured for meltwater volume after natural melting, and transferred to the same size polyethylene bottles. All the collected water samples were stored in a refrigerator at 0°C before testing.

Precipitation sample analysis from 2010 to 2013 was conducted using a Liquid Water Isotope Analyzer (DLT-100, Model: 908-0008) from Los Gatos Research, USA; subsequently, a new generation Liquid and Gas Dual-Mode Stable Isotope Analyzer (IWA-35EP, Model: 912-0026-1000) from the same company was used from 2014 to

215 2022. The oxygen and hydrogen stable isotope ratio in the water samples were

216 expressed in per mil (‰) deviations relative to the Vienna Standard Mean Ocean Water

217 (V-SMOW), calculated using the equation:

$$\delta^2\text{H or } \delta^{18}\text{O} = \left[R_s \middle/ R_{\text{V-SMOW}} - 1 \right] \times 1000 \qquad (1)$$

219 In the equation, R_s and $R_{\text{V-SMOW}}$ represent the oxygen (or hydrogen) stable isotope ratios

220 $^{18}\text{O}/^{16}\text{O}$ (or $^2\text{H}/^1\text{H}$) in the water sample and in Vienna Standard Mean Ocean Water (V-

221 SMOW), respectively. The testing precision averaged $\delta^{18}\text{O} \leq 0.3‰$ and $\delta^2\text{H} \leq 2‰$

222 during 2010-2013, and $\delta^{18}\text{O} \leq 0.2‰$ and $\delta^2\text{H} \leq 0.6‰$ during 2014-2022. If there were

223 two precipitation samples in one day, the precipitation stable isotope values for that day

224 were represented by the volume-weighted average. In total, 1668 precipitation days'

225 $\delta^{18}\text{O}$ ($\delta^2\text{H}$) data were obtained over the past 13 years.

226 **2.3 Ancillary data**

227 ERA5, produced and released by the European Centre for Medium-Range Weather

228 Forecasts (ECMWF), is the fifth-generation global atmospheric reanalysis data product

229 from the center. Compared to its predecessor ERA-Interim, ERA5 incorporates a state-

230 of-the-art integrated forecasting system, integrates more historical observational data,

231 and reprocesses a large amount of assimilation data, resulting in significantly improved

232 accuracy (Albergel et al., 2018; Hoffmann et al., 2019). Additionally, ERA5 features

233 substantial improvements in temporal and spatial resolution. The temporal resolution

234 has increased from 6 hours in ERA-Interim to 1 hour, while the horizontal resolution

235 has improved from 79 km to 31 km, and the highest vertical extension reaches 0.01 hPa

236 level. These enhancements enable ERA5 to capture finer atmospheric details. Moreover,

237 the number of variables provided by ERA5 has increased from over 100 in ERA-Interim

238 to the current 240, and the release delay days of ERA5 have been reduced from 2-3

239 months in ERA-Interim to 5 days (Albergel et al., 2018; Hoffmann et al., 2019). The

240 reanalysis data (January 1979 to December 2017, totaling 468 months) used in this

241 study include surface pressure (p_s, hPa), potential height of 500 hPa (H_{500}, meter), and

242 specific humidity (q, kg·kg^{-1}), latitudinal wind (m/s), and meridional wind (m/s) at

243 1000/850/700/600/500/400/300 hPa. The horizontal resolution is 1°×1°, with a

244 temporal step of 1 hour. This dataset was used to calculate the vertical integral of water

245 vapor fluxes into a specified region, introduced in section 2.4.

246   Since the direct observation of the isotopic fractionation process in the atmosphere

247 is extremely challenging, analyzing the variations of atmospheric stable isotopes

248 requires the application of stable isotopes fractionation theory along with the

249 fundamental principles and methods of meteorology. In terms of research methods, the

250 introduction of atmospheric circulation models for water stable isotope cycling, such as

251 isoGCMs, provides a unique and effective tool. Among numerous isoGCMs, isoGSM

252 (Isotope-incorporated Global Spectral Model) exhibits relatively good simulation

253 performance in the East Asian region (Zhang et al., 2020; Kathayat et al., 2021).

254 isoGSM is a stable isotope GCM developed by Yoshimura et al. (2008), which

255 integrated water isotope cycling and fractionation processes into the Global Spectral

256 Model at the Scripps Experimental Climate Prediction Center. The driving data include

257 sea surface temperature, sea ice, and temperature and horizontal wind fields in 28

258 vertical layers. This model addresses the Gibbs phenomenon in atmospheric circulation

models and performs better in simulating water vapor transport processes in arid and high-altitude regions (Yoshimura et al. 2008; Bong et al., 2024). The second-generation isoGSM2 has a higher temporal and spatial resolution in simulating water vapor and precipitation isotopes compared to the first-generation (Chiang et al., 2020). It utilizes the NECP-R2 (National Centers for Environmental Prediction Reanalysis 2) reanalysis dataset and abandons the NDSL (Non-iteration Dimensional-split Semi-Lagrangian) advection scheme used in the previous generation. By dynamically correcting the model output using reanalysis data, isoGSM2's simulation results are closer to actual atmospheric conditions, thereby improving the accuracy of water vapor and precipitation isotope simulations (Bong et al., 2024).

The water stable isotope simulation data used in this study are from isoGSM2 (January 1979 to December 2017, totaling 468 months), including monthly precipitation amount (P, mm), stable isotopes (δ^2H and $\delta^{18}O$) in the precipitation (δ^2H_p, $\delta^{18}O_p$), the ~~and~~ vertical integral of water vapor isotopes (δ^2H_v, and $\delta^{18}O_v$) of 17 pressure levels from 1000 hPa to 10 hPa ~~(δ^2H_p, $\delta^{18}O_p$, δ^2H_v, and $\delta^{18}O_v$)~~, and the calculated deuterium excess in water vapor and precipitation (~~Ex~~ d_v and ~~Ex~~ d_p). The spatial scale ranges from 30°S to 70°N and 0° to 280°E, with a horizontal resolution of 1°×1° (Chiang et al., 2020; Liu et al., 2023).

2.4 Calculation of the Vertical Integral of Water Vapor Flux Q

The water vapor transport flux serves as a metric for both the magnitude and direction of water vapor transport, representing the mass of water vapor passing through a unit cross-section per unit of time (Sun et al., 2011). The specific calculation equation

is as follows:

$$Q = \frac{1}{g} \int_{p_t}^{p_s} V q \, \mathrm{d}p \qquad (2)$$

Where the meridional component Q_λ and the latitudinal component Q_φ of the water vapor transport flux are given by:

$$Q_\lambda = \frac{1}{g} \int_{p_t}^{p_s} u q \, \mathrm{d}p \qquad (3)$$

$$Q_\varphi = \frac{1}{g} \int_{p_t}^{p_s} v q \, \mathrm{d}p \qquad (4)$$

Here, Q represents the vertical integral of water vapor flux ($kg \cdot m^{-1} \cdot s^{-1}$), including the meridional component Q_λ and the latitudinal component Q_φ. V denotes the vector wind speed ($m \cdot s^{-1}$), including the latitudinal wind speed (v) and meridional wind (u), q represents specific humidity ($kg \cdot kg^{-1}$), g is the acceleration due to gravity ($m \cdot s^{-2}$), p_s is the lower boundary pressure (hPa), and p_t is the upper boundary pressure (hPa). In the actual atmosphere, water vapor content above 300 hPa is minimal, thus p_t is set to 300 hPa when calculating the vertical integral of water vapor flux through the entire atmospheric column.

3. Results

3.1 Seasonal Variation Characteristics of Precipitation Isotopes in the Changsha Region

The monthly weighted average and total monthly calculations were performed on the daily $\delta^{18}O_p$, daily ~~Ex~~ d_p, and daily P collected from the Hunan Normal University and the Changsha National Meteorological Reference Station, yielding the seasonal variations of multi-year monthly weighted average $\delta^{18}O_p$, monthly weighted average

302 ~~Ex~~ d_p, and monthly average P in the Changsha region (Fig. 2a). The $\delta^{18}O_p$, ~~Ex~~ d_p, and

303 P in Changsha exhibited significant seasonal variations—that is, the maximum value

304 of $\delta^{18}O_p$ appeared in March and April, both at −3.6‰, but did not correspond to the

305 months with the lowest precipitation amounts. The three lowest values of $\delta^{18}O_p$

306 occurred in July, August, and September, respectively at −9.5‰, −8.9‰, and −9.4‰,

307 with a simple arithmetic average of −9.3‰, which also did not correspond to the months

308 with the highest precipitation amounts. The maximum value of ~~Ex~~ d_p (20.1‰)

309 appeared in January, and the minimum value (9.3‰) appeared in August, both of which

310 were months with relatively low precipitation. Due to these significant differences in

311 the phases of precipitation isotopes and amounts, it is apparent that explaining the

312 variations in local precipitation stable isotopes solely based on the seasonal variations

313 in local precipitation amounts is insufficient.

314
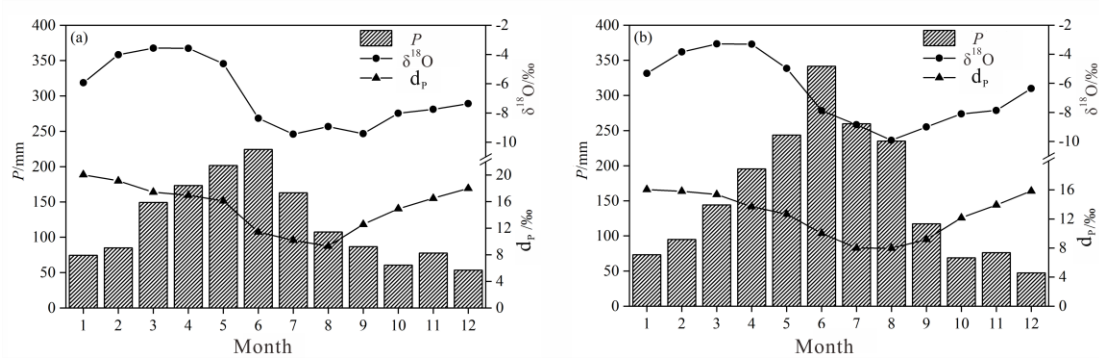
315 Fig. 2 Comparisons between seasonal variations of precipitation $\delta^{18}O$ ($\delta^{18}O_p$),

316 precipitation deuterium excess (~~Ex~~ d_p), and precipitation amount (P) measured at the

317 Changsha station (a) and simulated by isoGSM2 or driven from the ERA5 reanalysis

318 dataset at the corresponding grid (b).

319 Monthly weighted average calculation was performed on the monthly $\delta^{18}O_p$ and

320 ~~Ex~~ d_p simulated by isoGSM2 at the Changsha grid, and the monthly average

calculation was performed on the P from ERA5, yielding the seasonal variations of simulated monthly weighted average $\delta^{18}O_p$ and ~~Ex~~ d_p and ERA5 monthly average P at the Changsha grid (Fig. 2b). The simulated and calculated $\delta^{18}O_p$, ~~Ex~~ d_p, and P in Changsha all effectively reproduced the seasonal variations of the corresponding observations. The root mean square errors (RMSE) between simulated and observed values were 0.5‰, 2.8‰, and 59.7 mm, respectively. Corresponding to the observed seasonal variations, the two maximum values of the simulated $\delta^{18}O_p$ occurred in March and April, at −3.3‰ and −3.3‰, respectively, with very small differences from the observed values. The three lowest values of simulated $\delta^{18}O_p$ also occurred in July, August, and September, at −8.8‰, −9.9‰, and −9.0‰, respectively, with a simple arithmetic average of −9.3‰, which was consistent with the observed values. The maximum value of simulated ~~Ex~~ d_p (16.1‰) appeared in January, and the minimum value (8.0‰) appeared in August (Fig. 2b), both consistent with the observed values (Fig. 2a). These comparisons indicated that isoGSM2 exhibited strong capabilities in simulating the temporal variations of atmospheric water stable isotopes.

To analyze the seasonal variation in the atmospheric water vapor transport and its influences on the regional precipitation isotopes, and taking into account the hydro-climatic characteristics of the study region (Fig. 2), four representative months including January, April, June, and October were selected as the study seasons. Among these representative months, January in the Changsha region represents winter, characterized by the lowest temperatures and relatively low precipitation throughout the year. April signifies spring, with rapidly increasing precipitation amounts and

343   frequent fluctuations between warm and cold air masses. June represents the peak of

344   the summer monsoon season, with the highest monthly precipitation amount of the year.

345   October represents autumn, characterized by clear and cool weather and the second-

346   lowest precipitation throughout the year under the influence of the West Pacific

347   Subtropical High.

348   **3.2 Water Vapor Transport in the Dongting Lake Basin in Different Seasons**

349   **3.2.1 Average Water Vapor Transport Path in the Dongting Lake Basin in January**

350   Based on the ERA5 reanalysis data, we calculated and plotted the spatial

351   distribution of the 500 hPa average geopotential height (H_{500}) and average Q (Fig. 3a),

352   multi-year average P (Fig. 3b) in January. Moreover, based on the isoGSM2 simulation

353   data, we plotted the spatial distributions of the average $\delta^{18}O_v$ (Fig. 3c), $\delta^{18}O_p$ (Fig. 3d),

354   ~~Ex~~ d_v (Fig. 3e), and ~~Ex~~ d_p (Fig. 3f) in January.
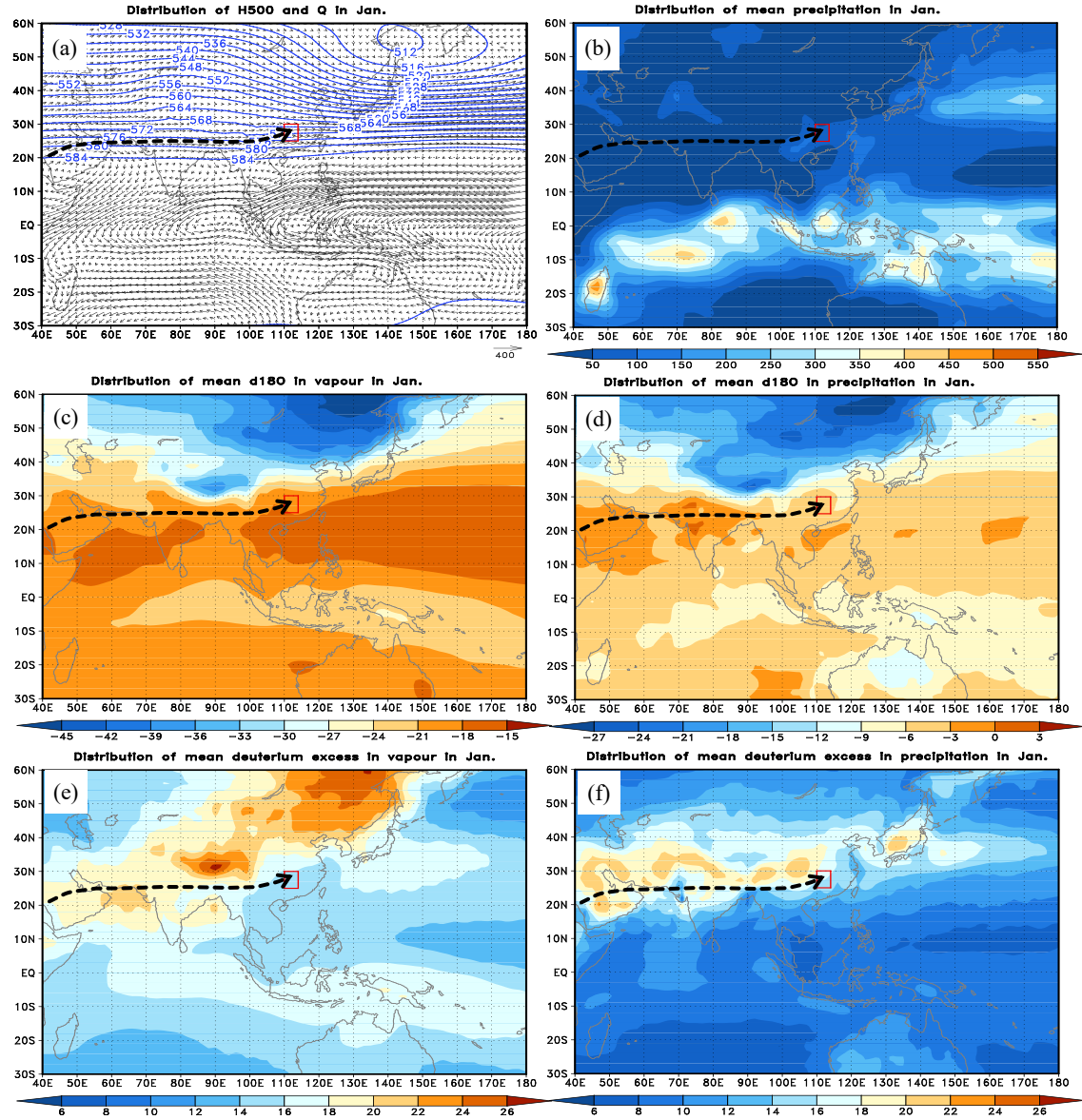
Fig. 3 Mean vapor transport path to the Dongting Lake Basin and the spatial

distributions of Q with H_{500} (a), P (b), $\delta^{18}O_v$ (c), $\delta^{18}O_p$ (d), ~~Ex_~~d_v (e), and ~~Ex_~~d_p (f) in

January. Q, H_{500}, P, $\delta^{18}O_v$, $\delta^{18}O_p$, ~~Ex_~~d_v, and ~~Ex_~~d_p represent the vertical integral of

water vapor flux, 500 hPa average geopotential height, precipitation amount, $\delta^{18}O$ in

atmospheric water vapor and precipitation, and deuterium excess in atmospheric

water vapor and precipitation, respectively, hereinafter the same.

At the H_{500} field of East Asia, the deep East Asian Trough was stably located along

the East coast, and the strong Ural Ridge in the mid-high latitudes of 70°E to 90°E (Fig.

3a). Influenced by the northwest airflow behind the trough and ahead of the ridge, the northwest winds prevailed in most parts of East Asia. In the Dongting Lake Basin (highlighted in the red box in Fig. 3), influenced by the middle-latitude westerly belt, water vapor transport mainly was from west to east. Under the control of the cold continental high, precipitation was relatively low over the entire East Asia and South Asia, while the regions with high P values were mainly distributed in the equatorial convergence zone and the North Pacific located ahead of the East Asian Trough (Fig. 3b). Unlike most regions of the East Asian continent, the Dongting Lake Basin was situated on a wet tongue, benefiting from the Southwest Vortex in the eastern Tibetan Plateau (Lai et al., 2023; Huang and Li, 2023). This Southwest Vortex is a cyclonic bypass flow of westerlies from the southern branch of the Tibetan Plateau, as this vortex moves eastward with the westerly belt, it brings precipitation to the downstream areas

The $\delta^{18}O_v$ and $\delta^{18}O_p$ in January exhibited significant continental effects (Figs. 3c and 3d). Under the control of continental cold air masses, the centers of minimum $\delta^{18}O_v$ and $\delta^{18}O_p$ values were located in the mid-high latitudes of Eastern Siberia. Due to the influence of topography, the $\delta^{18}O_v$ tended to be negative over the Tibetan Plateau. These two low-value regions correspond to the cold pole of Eurasia and the Earth's third pole, respectively. Regions enriched in atmospheric water isotopes were mainly distributed over vast oceans and Western Asia. In the equatorial convergence zone, due to the rainout effects, both water vapor isotopes and precipitation isotopes were depleted to some extent. Along with the surrounding the Dongting Lake Basin, the abundance of water vapor isotopes and precipitation isotopes in the Dongting Lake Basin were

comparable to those of the middle-low latitude oceans in January.

The spatial distributions of the ~~Ex~~ d_v and ~~Ex~~ d_p exhibited the characteristics of low in the ocean and high in the land, but the regions where their maximum values occurred did not completely correspond (Figs. 3e and 3f). The maximum value of the ~~Ex~~ d_v mainly appeared in Eastern Siberia and the Tibetan Plateau, showing a meridional distribution from northeast to southwest, while the high values of the ~~Ex~~ d_p mainly occurred in mid-latitude inland regions, showing a latitudinal distribution from west to east. The ~~Ex~~ d_v and ~~Ex~~ d_p values in the Dongting Lake Basin lay exactly in the transition region from low to high values. Typically, the ~~Ex~~ d_p largely depended on the ~~Ex~~ d_v, but processes such as condensation and super-saturation in ice-water mixed clouds, secondary evaporation below clouds, evaporation from underlying surfaces, and the exchange and diffusion of water vapor isotopes could cause precipitation isotopes to deviate to varying degrees from atmospheric water vapor isotopes (Zhang et al., 2016).

In the Q field (Fig. 3a), regarding the Dongting Lake Basin (represented by the red box) as the endpoint, the vector cluster of the vertical integral of water vapor flux (i.e., the Q) directed towards the Dongting Lake Basin delineates the path of water vapor transport in January (black arrow lines in Fig. 3). The water vapor transport paths were determined by identifying systematic vapor currents in the Q field~~The water vapor transport path was determined by the rules to find the systematic vapor currents in the~~ ~~Q field~~, which need to have the same directionality and draw the path along the central axis of the vapor currents. Our identified water vapor transport paths are conceptually

similar to atmospheric rivers, which are long, narrow corridors of strong horizontal water vapor transport typically associated with low-level jets (Ralph et al., 2017; Payne et al., 2020). However, our paths are derived from the climatological mean state (multi-year monthly averages) rather than short-term events, which is a key distinction from atmospheric rivers that generally last for a few days to a week (Dettinger et al., 2013).

The source regions of water vapor were determined based on the conditions for the formation of air masses, which need to form on a uniform underlying surface and possess stably stability and similarity in terms of isotopic, thermodynamic, and dynamic properties as well as circulation conditions, typically located over vast land and ocean regions (Smirnov and Moore, 1999). These regions are typically located over vast land and ocean areas and serve as the starting points of the water vapor transport paths. Although there is some empiricism and subjectivity, there is no explicit algorithm to determine the exact water vapor transport path and source regions of water vapor. However, this approach is based on certain criteria and ensures that we capture the systematic vapor currents that have the most significant influence on the local precipitation and its isotopic composition, and it provides a reasonable basis for identifying the dominant vapor transport directions and the primary sources of water vapor contributing to precipitation in the Dongting Lake Basin.

The westerly path is considered dominant because it represents the primary direction of water vapor convergence towards the Dongting Lake Basin, as indicated by the strongest and most consistent flux vectors in the Q field. The selection of this path is based on the physical significance of the Q field, which integrates both the

magnitude and direction of water vapor transport and reflects the dominant atmospheric

circulation pattern influencing the region in this season. This transport path originated

near the Arabian Peninsula. Driven by the southern branch of the westerly stream jet on

the southern side of the Tibetan Plateau, water vapor transported along the southern

side of the Tibetan Plateau, passed through southwestern China via the northern part of

the Indian Peninsula, and reached the Dongting Lake Basin. Moreover, It it can be seen

that this water vapor transport path was not consistent with the prevailing wind direction

in January as shown in Fig. 1a, which was represented by the black arrows with

northwesterly winds prevailing in the Dongting Lake Basin as shown by the average

wind field at the 850 hPa.

In analyzing the variations along the water vapor transport paths, we selected

several points along the path from the source region to the Dongting Lake Basin, spaced

at nearly equal intervals (Fig. 4). Six series of factors at the grid points along the water

vapor transport path were derived from each factor field in January, including the

variations of Q, P, $\delta^{18}O_v$, $\delta^{18}O_p$, Ex d_v, and Ex d_p., these points allow us to examine

the changes in these factors along the transport path. Moreover, the grid points along

the water vapor transport path were identified on the central axis of the path and based

on the principle of uniform distribution of the scatter points, and the factors at the grid

points were obtained from these scatter points. Besides, the factors at the grid points

along the water vapor transport path exhibit, in spatial terms, average characteristics of

conditions over multiple years, and, in temporal terms, sequential characteristics of

these factors along the water vapor transport path. As shown in Fig. 4, both the Q and

452   *P* were relatively low, while increased to some extent due to the converging effect of

453   Southwest Vortex after entering the Dongting Lake Basin (Figs. 4a and 4b). Under the

454   weak atmospheric meridional disturbances in January, the changes in $\delta^{18}O_v$ and ~~Ex~~ d_v

455   were minor, fluctuating slightly around −19.1‰ and 18.2‰, respectively (Figs. 4c and

456   4e). Due to the low precipitation amount, the $\delta^{18}O_p$ values were higher in the first half

457   of the water vapor transport path, and then became more negative in the latter half with

458   the enhanced rainout effect, while the ~~Ex~~ d_p became more positive (Figs. 4d and 4f).

459
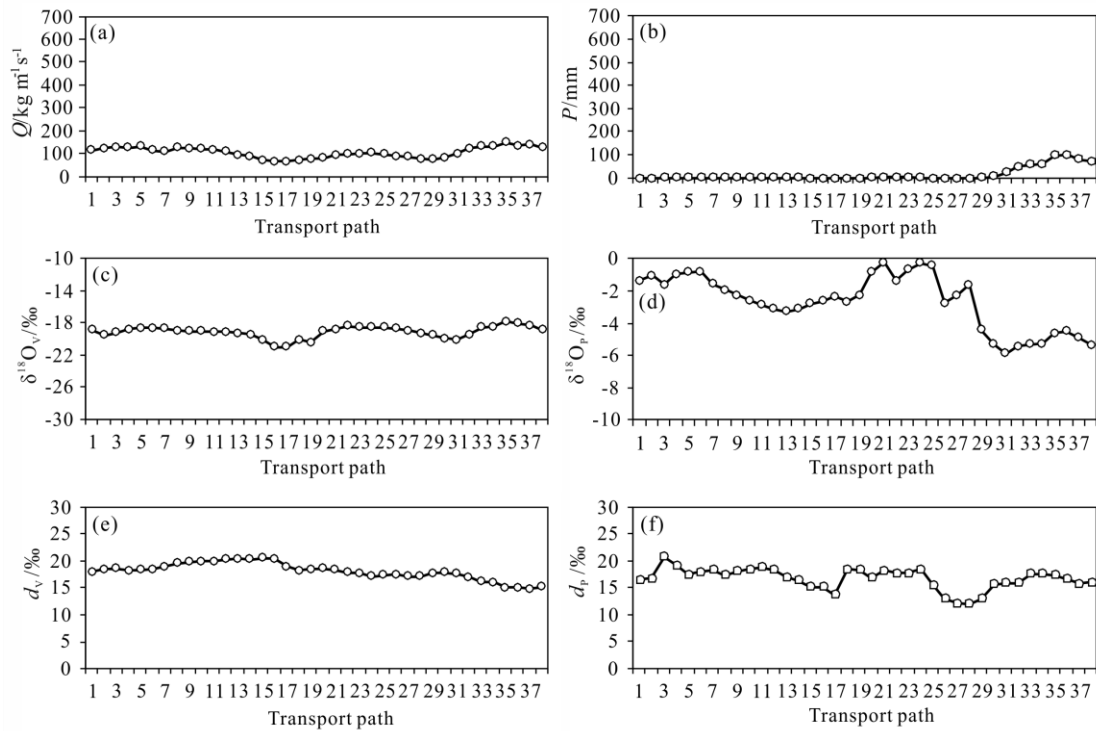
460   Fig. 4 Mean variations of Q (a), P (b), $\delta^{18}O_v$ (c), $\delta^{18}O_p$ (d), ~~Ex~~ d_v (e), and ~~Ex~~ d_p (f)

461   along the vapor transport path in January. The numbers at the lower axis represent the

462   serial numbers corresponding to the grid points along the water vapor transport path

463   from the source region to the Dongting Lake Basin, and the points along the path were

464   selected at almost equal intervals to capture the variations of each factor, hereinafter

465   the same.

3.2.2 Average Water Vapor Transport Path in the Dongting Lake Basin in April

Based on the ERA5 reanalysis data and the isoGSM2 simulation data, the spatial distributions of H_{500}, Q, P, $\delta^{18}O_v$, $\delta^{18}O_p$, ~~Ex~~ d_v, and ~~Ex~~ d_p were calculated and plotted in April (Fig. 5). At the H_{500} field (Fig. 5a), the East Asian Trough and Ural Ridge were still present in the mid-to-high latitudes. The mid-to-high latitude regions of East Asia were still influenced by the winter monsoon, while its intensity was significantly weakened. In the mid-to-low latitudes, the Western Pacific subtropical high has strengthened and expanded northward, with the ridge line located approximately near 15°N. A shallow trough appeared in the northern part of the Bay of Bengal, indicating the beginning of tropical systems influencing the mid-to-low latitude regions of East Asia. In the Dongting Lake Basin, influenced by the westerlies and low-latitude atmospheric systems, the water vapor transport shifted to the domination by the southwestward direction. Most continental regions of East Asia and South Asia experienced a certain degree of precipitation increase, with the rainy band caused by the intertropical convergence zone, previously located in the Southern Hemisphere, moving to the Northern Hemisphere (Fig. 5b). The Dongting Lake Basin also entered the spring flood season in April, while the Changsha region was situated in a center with an above-average spring precipitation amount compared to the surrounding regions in this period (Fig. 5b).
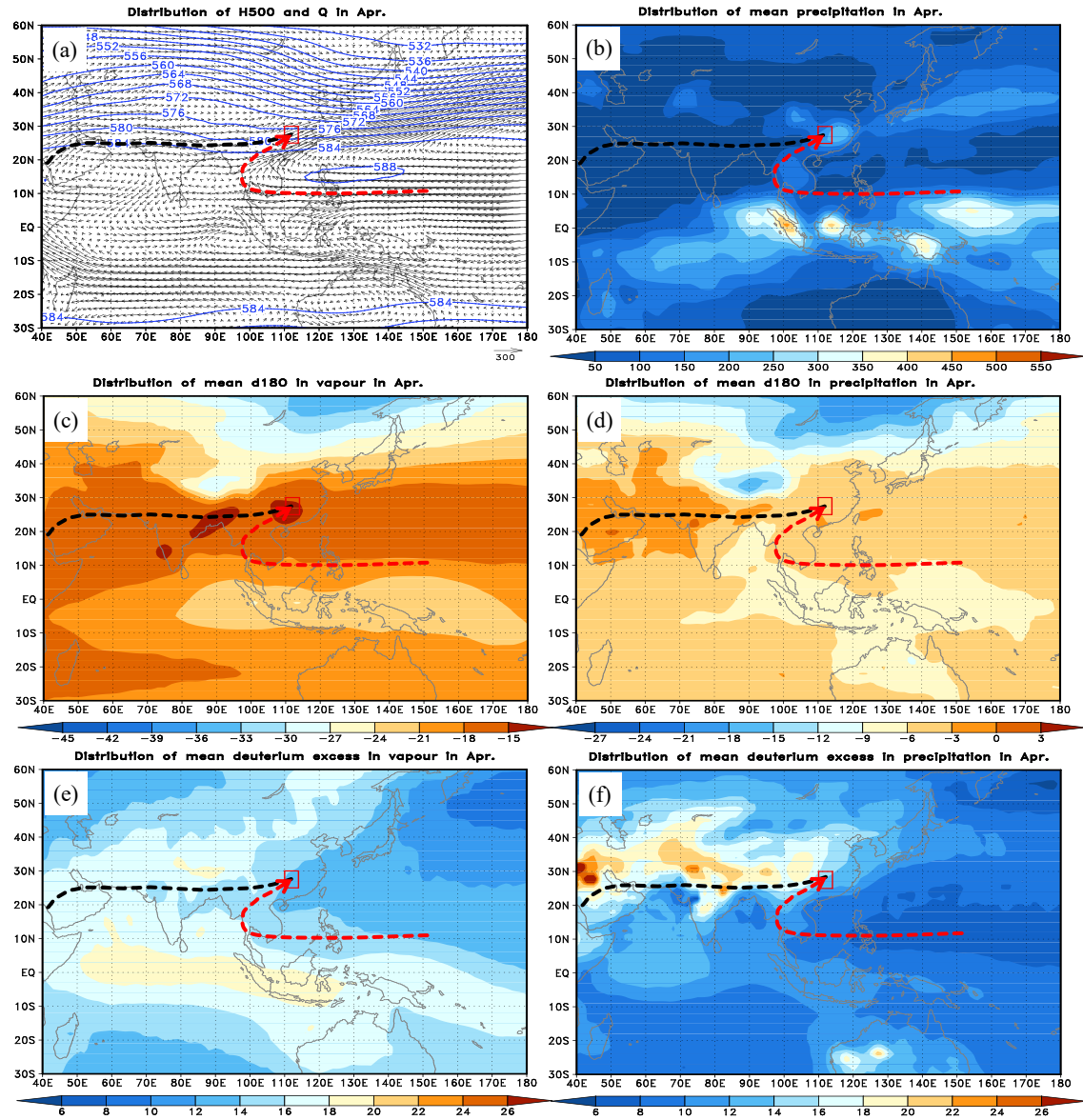
Fig. 5 Mean vapor transport paths to the Dongting Lake Basin and the spatial

distributions of Q with H_{500} (a), P (b), $\delta^{18}O_v$ (c), $\delta^{18}O_p$ (d), ~~Ex_~~d_v (e), and ~~Ex_~~d_p (f) in

April.

Compared to the situations in January, there were no major changes in the spatial

distributions of $\delta^{18}O_v$ and $\delta^{18}O_p$ in April (Figs. 5c and 5d). In the regions with low $\delta^{18}O_v$

and $\delta^{18}O_p$ values, previously located in Eastern Siberia and the Tibetan Plateau,

atmospheric stable isotopes have significantly enriched. Due to temperature rise and

enhanced evaporation, the regions with high levels of $\delta^{18}O_v$ and $\delta^{18}O_p$ in the mid-to-

494   low latitudes showed continual increases in the $\delta^{18}O_v$ and $\delta^{18}O_p$ values. With the

495   strengthening of water vapor convergence in the Dongting Lake Basin, the $\delta^{18}O_v$ in the

496   Dongting Lake Basin showed significant increases in April, leading to an isotopic

497   enrichment in precipitation. Compared to the large-scale region, the water isotope

498   composition in the Dongting Lake Basin, was not significantly different from that of

499   the mid-to-low latitude ocean, indicating the controls by the oceanic air masses (Figs.

500   5c and 5d).

501   In April, the spatial distributions of ~~Ex~~ d_v and ~~Ex~~ d_p were comparable to the

502   situations in January (Figs. 5e and 5f). The regions with high-value ~~Ex~~ d_v, previously

503   located in Eastern Siberia and the Tibetan Plateau, respectively, showed significant

504   reductions in range and intensity, but the regions with low-value ~~Ex~~ d_v in the Western

505   Pacific expanded, thereby reducing the differences between land and sea. With the

506   continuous inland influx of oceanic water vapor from the Western Pacific Ocean, the

507   range of low-value regions of the ~~Ex~~ d_p has expanded. ~~Influencing~~ Influenced by the

508   increasing precipitation, the range of high-value regions of the ~~Ex~~ d_p in mid-latitude

509   inland regions has narrowed, but the intensity has increased to varying degrees,

510   especially in West Asia. Finally, both the ~~Ex~~ d_v and ~~Ex~~ d_p in the Dongting Lake Basin

511   showed decreases, which were influenced by the gradually strengthening summer

512   monsoon and the situation of water vapor transport (Figs. 5e and 5f).

513   Two water vapor transport paths were obtained according to the vector

514   interpolation method introduced in section 3.2.1 (Fig. 5a). The first water vapor

515   transport path—that is, Path I (represented by black arrow lines in Fig. 5), was

516 essentially consistent with the water vapor transport path in January, but it is slightly

517 shifted northward by one degree of latitude. The second water vapor transport path—

518 that is, Path II (represented by red arrow lines in Fig. 5), driven by the weak Western

519 Pacific subtropical high, guided warm and moist water vapor from the low latitudes of

520 the Western Pacific along the outer edge of the subtropical high, passing through the

521 South China Sea and the Indochinese Peninsula and finally reached into the Dongting

522 Lake Basin. Corresponding data at the grid points along two water vapor transport paths

523 were extracted and plotted for the Q, P, $\delta^{18}O_v$, $\delta^{18}O_p$, ~~Ex~~ d_v, and ~~Ex~~ d_p (Fig. 6).

524
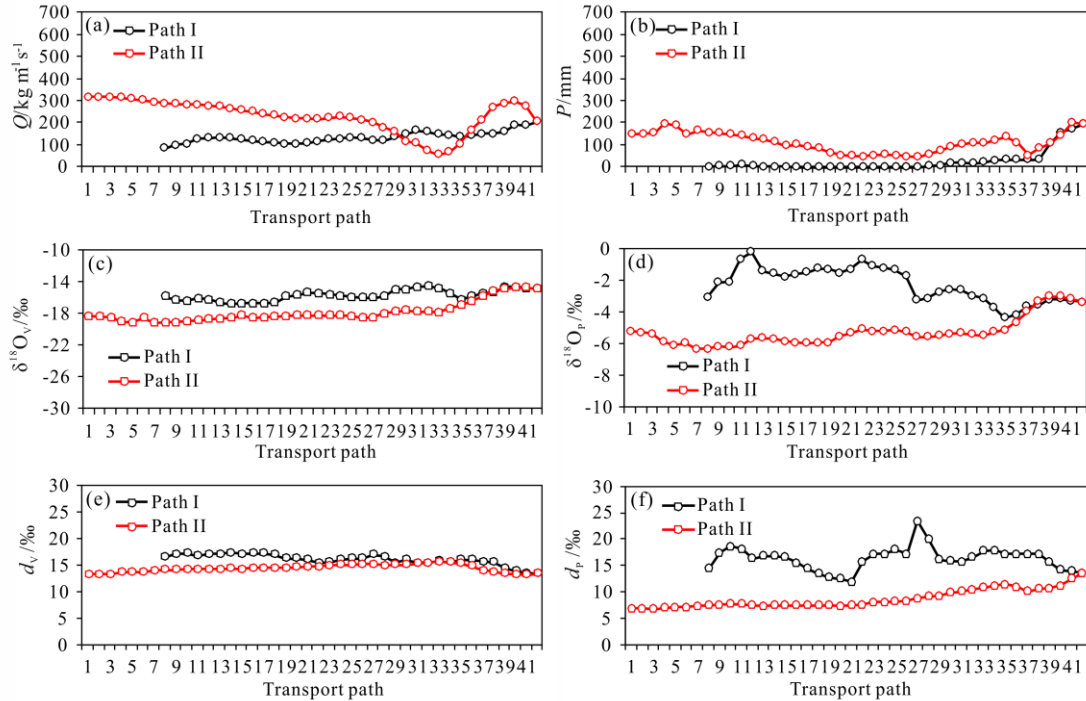
525 Fig. 6 Mean variations of Q (a), P (b), $\delta^{18}O_v$ (c), $\delta^{18}O_p$ (d), ~~Ex~~ d_v (e), and ~~Ex~~ d_p (f)

526 along the vapor transport paths in April.

527 Along Path I, both the Q and P showed slight increases compared to the situations

528 in January (Figs. 6a and 6b), with the average values in the first half of the water vapor

529 transport path before entering the Dongting Lake Basin were 128.2 kg m^{-1} s^{-1} and 10.5

mm, respectively, still at relatively low levels. After entering the Dongting Lake Basin, the average Q and P increased to 180.1 kg m^{-1} s^{-1} and 135.0 mm, respectively. Under the transport of latitudinal water vapor, the $\delta^{18}O_v$ increased slightly from −15.8‰ to −14.9‰, while the $\delta^{18}O_p$ decreased slightly from −2.1‰ to −3.3‰ (Figs. 6c and 6d). The corresponding ~~Ex~~ d_v decreased from 16.5‰ to 14.3‰, and the ~~Ex~~ d_p decreased from 16.6‰ to 15.0‰, indicating the input of oceanic water vapor (Figs. 6e and 6f).

Along Path II, both the Q and P were significantly larger than those along the latitudinal Path I (Figs. 6a and 6b), with the average values before entering the Dongting Lake Basin were 226.6 kg m^{-1} s^{-1} and 108.2 mm, respectively. After entering the Dongting Lake Basin, these values increased to 269.2 kg m^{-1} s^{-1} and 148.6 mm, respectively. The area where Q decreased significantly corresponds to a water vapor divergence region at the southwest corner of the Indochinese Peninsula. Under the meridional water vapor transport, the $\delta^{18}O_v$ increased from −18.2‰ to −14.9‰, while the $\delta^{18}O_p$ from −5.5‰ to −3.2‰ (Figs. 6c and 6d); correspondingly, the ~~Ex~~ d_v decreased from 14.6‰ to 13.5‰, while the ~~Ex~~ d_p increased from 8.3‰ to 11.8‰ (Figs. 6e and 6f), following the variation rule of deuterium excess during water vapor transport—that is, as the rainout effect progressed, the heavier isotopes preferentially left the water vapor parcel or cloud during the water vapor transport processes and generated precipitation, thus resulted in subsequent precipitation having increasingly higher deuterium excess values (Vasil'chuk, 2014). Moreover, there was a large increase in both the Q and P before entering the Dongting Lake Basin along Path II, and the increase in the isotope ratio of precipitation may seem inconsistent with the

rainout effect, which typically leads to the depletion of heavier isotopes in the remaining water vapor. However, this increase can be attributed to the horizontal convergence of more enriched water vapor. Path II showed a significant increase in both the Q and P before entering the Dongting Lake Basin (Fig. 6a). This suggested that the enriched water vapor from the surrounding water vapor contributed to the overall increase in the $\delta^{18}O_v$ and $\delta^{18}O_p$. The influx of this enriched water vapor counteracts the depletion effect caused by rainout, resulting in the observed increase in precipitation isotope values.

3.2.3 Average Water Vapor Transport Path in the Dongting Lake Basin in June

Based on the ERA5 reanalysis data and isoGSM2 simulation data, the spatial distributions of the average H_{500}, Q, P, $\delta^{18}O_v$, $\delta^{18}O_p$, Ex d_v, and Ex d_p were respectively calculated and plotted in June (Fig. 7). At the H_{500} field (Fig. 7a), the East Asian Trough continues to stably exist in June, but the position of trough line shifted eastward over the North Pacific Ocean. The high-pressure ridge in the eastern part of the Ural Mountains weakened and shifted eastward over Lake Baikal. The rapidly intensifying western Pacific subtropical high expanded westward and northward, with its ridge line located at approximately 22~23°N, while the India-Burma Trough in the northern Bay of Bengal strengthened continuously. The atmospheric circulation conditions indicated that most of East Asia, including the south of the Yangtze River, has entered the prevailing period of summer monsoon (Fig. 7a). The warm and moist water vapor from the Arabian Sea and the Bay of Bengal driven by the India-Burma Trough as well as along the outer edge of the subtropical high from the western Pacific met the cold air moving southward behind the East Asian Trough and thus generated an

574 extremely long rain belt spanning 20 degrees of latitude and 70 degrees of longitude

575 from India, through the Indochinese Peninsula, to southern China until central Japan

576 (Fig. 7b). In this rain belt, the three largest precipitation centers were located on the

577 west coast of India, the Thai-Myanmar border region, and the Jiangnan region of China.

578 The formation of the first two precipitation centers was related to terrain, while the

579 formation of the precipitation center in the Jiangnan region of China was related to the

580 convergence of warm and moist water vapor from low latitudes to this region (Fig. 7b).

581
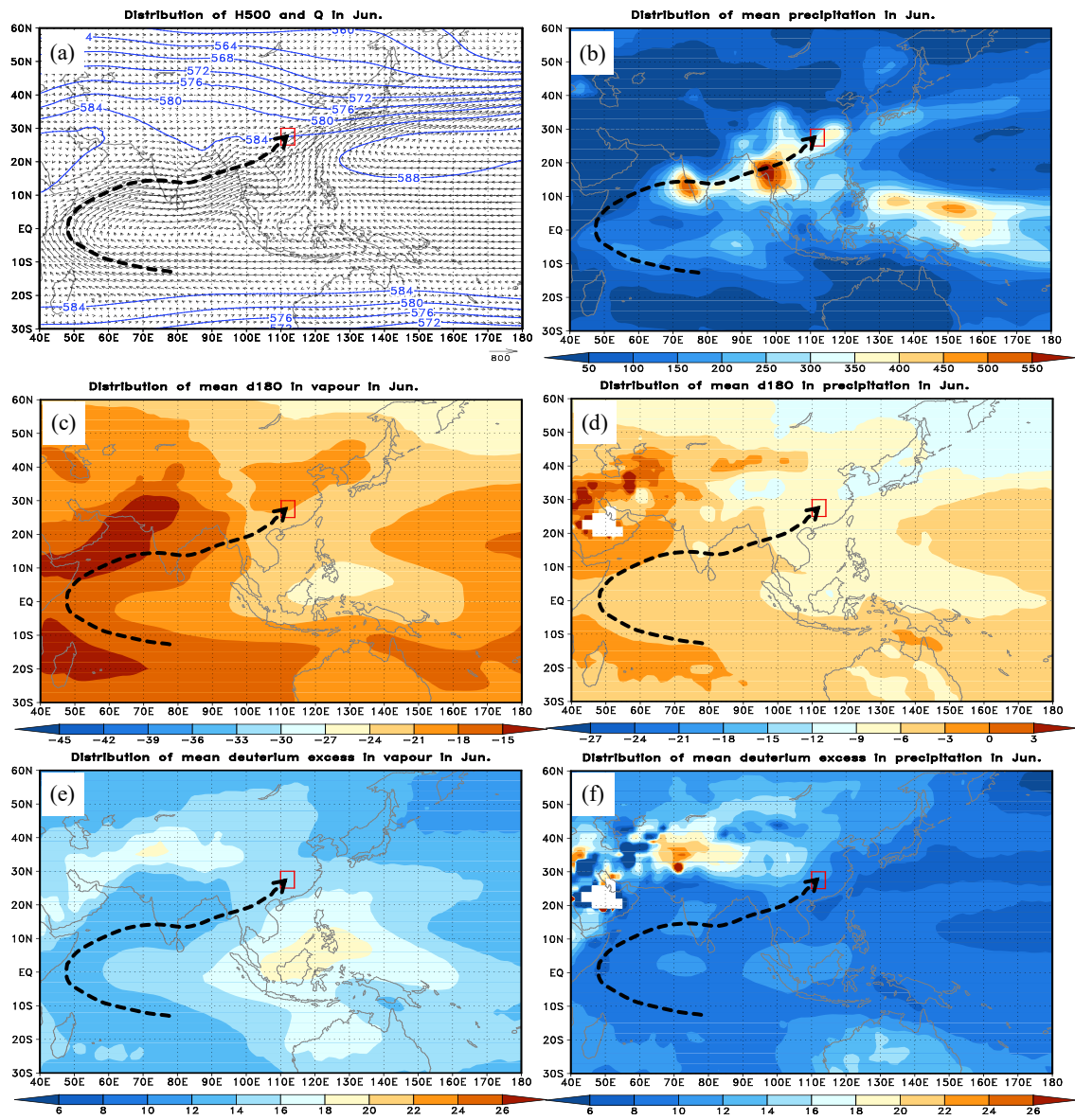
582 Fig. 7 Mean vapor transport path to the Dongting Lake Basin and the spatial

distributions of Q with H_{500} (a), P (b), $\delta^{18}O_v$ (c), $\delta^{18}O_p$ (d), ~~Ex~~ d_v (e), and ~~Ex~~ d_p (f) in

June.

With the change in circulation condition, the distributions of the $\delta^{18}O_v$ and $\delta^{18}O_p$

in June changed accordingly (Figs. 7c and 7d). The stable isotopes in both water vapor

and precipitation at mid-high latitudes were significantly enriched, with reduced spatial

differences. The $\delta^{18}O_v$ and $\delta^{18}O_p$ values remained high in the Arabian Sea, the Bay of

Bengal, and the Southern Ocean, the region with high $\delta^{18}O$ in the western Pacific

became narrowed, and the low $\delta^{18}O$ values in the Indonesia-Philippines region in the

western equatorial Pacific were associated with the enhanced water vapor convergence

(Figs. 7a, 7c, and 7d). The regional low $\delta^{18}O$ center previously present in the cold

season over the Tibetan Plateau had disappeared. In the Jiangnan region of China, the

convergence of water vapor from low-latitude oceans led to an isotopic enrichment in

water vapor, but the strong rainout effects caused an isotopic depletion in precipitation

(Figs. 7c and 7d). The spatial distributions of ~~Ex~~ d_v and ~~Ex~~ d_p in June showed no

significant differences compared to the situations in April (Figs. 5e, 5f, 7e, and 7f). The

high-value regions for the ~~Ex~~ d_v and ~~Ex~~ d_p were located in the region stretching from

western Asia through the Tibetan Plateau to southwestern China, as well as in the vast

oceanic region centered around the Philippines and Indonesia. Under the influence of

the summer monsoon, the difference in deuterium excess between East Asia and its

water vapor source—that is, the low-latitude ocean, remained relatively small (Figs. 7e

and 7f).

Based on the vector interpolation of the Q field (Fig. 7a), the water vapor transport

605   path was determined in June according to the vector interpolation method introduced

606   in Section 3.2.1 (shown by the black arrow lines in Fig. 7). This water vapor transport

607   path originated from the northern branch of the South Indian Ocean subtropical high,

608   crossed the equator, and transported through the Somali Sea, the Arabian Sea, the Indian

609   Peninsula, the Bay of Bengal, the Indochinese Peninsula, and entered the southwestern

610   region of China, finally reaching the Dongting Lake Basin. It can be seen that this water

611   vapor transport path was consistent with the prevailing wind direction in June as shown

612   in Fig. 1a. The corresponding Q, P, $\delta^{18}O_v$, $\delta^{18}O_p$, ~~Ex_~~d_v, and ~~Ex_~~d_p along the water

613   vapor transport path were extracted, and plotted in Fig. 8.

614
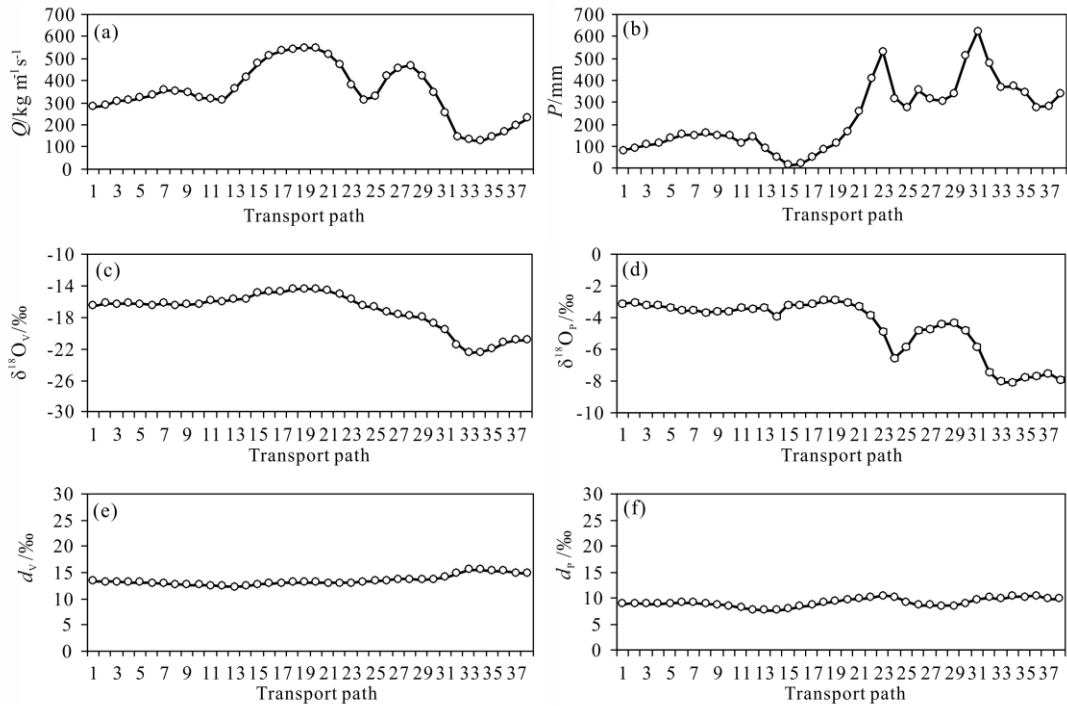
615   Fig. 8 Mean variations of Q (a), P (b), $\delta^{18}O_v$ (c), $\delta^{18}O_p$ (d), ~~Ex_~~d_v (e), and ~~Ex_~~d_p (f)

616   along the vapor transport path in June.

617   Along the water vapor transport path, the average Q and P were at their maximum

618   throughout the year, reaching 353.9 kg m^{-1} s^{-1} and 236.5 mm, respectively (Figs. 8a and

8b). The three extreme values of the Q along the transport path, or in the process of

transitioning from the maximum to minimum values, correspond to three P extremes

located at the western coast of the Indian Peninsula, the border region between Thailand

and Myanmar, and the region around the Dongting Lake Basin (Fig. 7b), with the values

of the three P extremes of 535.1 mm, 627.8 mm, and 341.5 mm, respectively (Fig. 8b).

With continuous precipitation especially after experiencing heavy precipitation and the

simultaneous persistent rainout processes, the stable isotopes in both water vapor and

precipitation exhibit a trend of continuous depletion (Figs. 8c and 8d). However, there

were no significant changes in both the ~~Ex~~ d_v and ~~Ex~~ d_p (Figs. 8e and 8f), the reasons

may be due to the continuous water vapor supply from low-latitude oceans, similar

advective paths between the grid points, and the similar degrees of sub-cloud

evaporation.

3.2.4 Average Water Vapor Transport Path in the Dongting Lake Basin in October

The spatial distributions of the average H_{500}, Q, P, $\delta^{18}Ov$, $\delta^{18}Op$, ~~Ex~~ d_v, and ~~Ex~~ d_p

in October were shown in Fig. 9. A notable feature at the H_{500} field in October was the

expansion of the latitudinal westerlies toward lower latitudes (Fig. 9a). In East Asia,

westerly winds prevail in the inland regions north of approximately 30°N, while much

of the regions south of 30°N were still influenced by the subtropical high-pressure

system. Compared to the peak period, the West Pacific subtropical high had

significantly weakened in autumn, and its main body had also retreated to the open sea.

However, a mesoscale anticyclone split from the high still controlled the Jiangnan

region of China including the Dongting Lake Basin, creating a climate characterized by

641   clear and crisp autumn (Fig. 9a). Due to the disappearance of the India-Burma Trough

642   and influenced by the anticyclone circulation, the water vapor transport from the

643   southwest low-latitude oceans decreased significantly. In the Dongting Lake Basin,

644   both the meridional and latitudinal water vapor transport were even less than the values

645   in January (Fig. 3a and 9a). Apart from the autumn rains in western China, precipitation

646   was generally scarce in East Asia in this period, with the rain belt shifting southward to

647   lower latitudes corresponding to the convergence zone near the equator, with the largest

648   precipitation regions located respectively south of the Equator in the Indian Ocean, the

649   Malay Peninsula, and north of the Equator in the western Pacific (Fig. 9b).
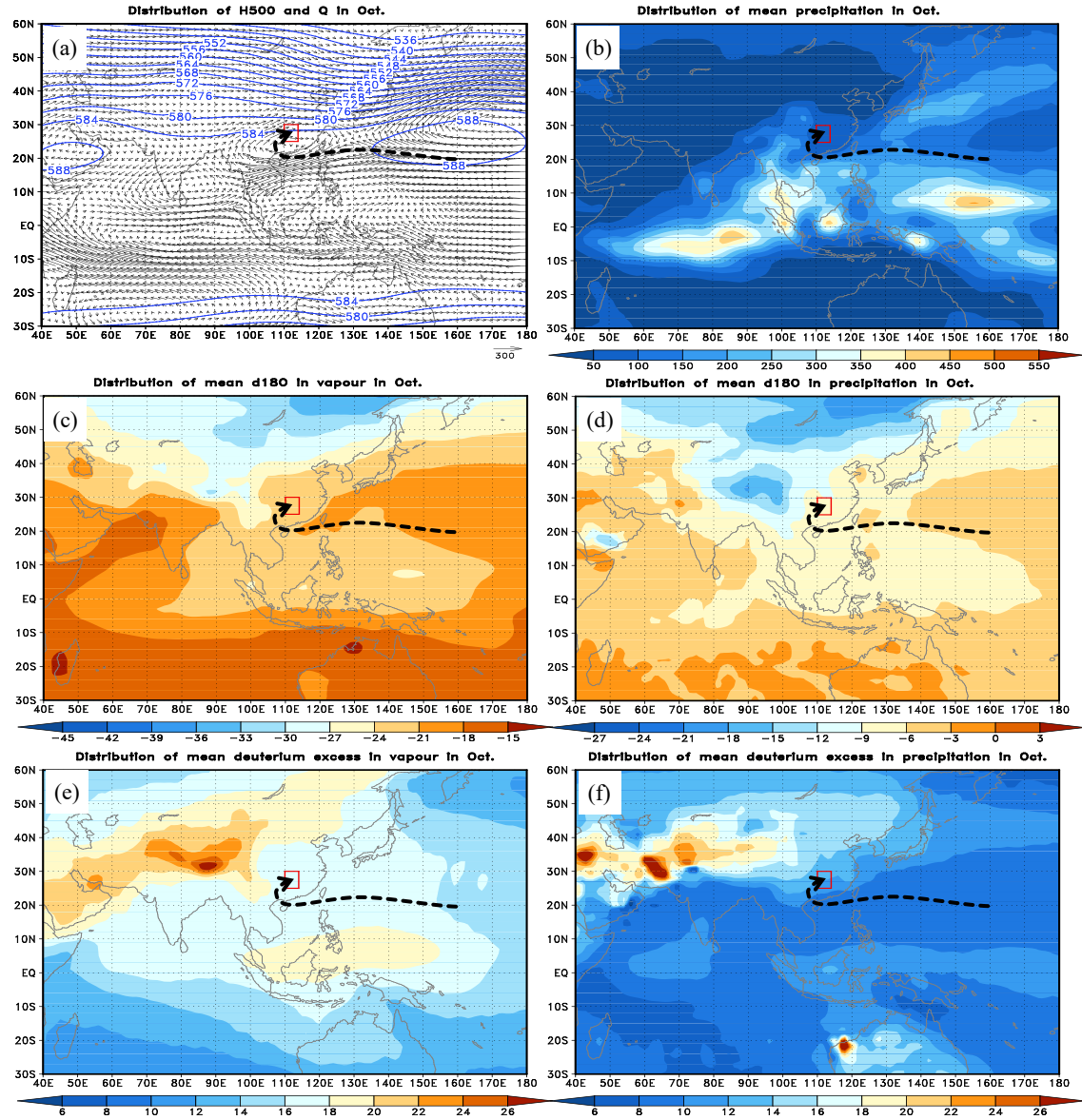
Fig. 9 Mean vapor transport path to the Dongting Lake Basin and the spatial

distributions of Q with H_{500} (a), P (b), $\delta^{18}O_v$ (c), $\delta^{18}O_p$ (d), ~~Ex_~~d_v (e), and ~~Ex_~~d_p (f) in

October.

Compared to the situations in June, there were no significant changes in the spatial

distribution of the $\delta^{18}O_v$ and $\delta^{18}O_p$ in October, but their differences between land and

sea as well as between high and low latitudes increased largely (Figs. 9c and 9d). The

stable isotopes in water vapor and precipitation were significantly depleted in Eastern

Siberia and the Tibetan Plateau, and accompanied by expansion of ranges. As a result,

the $\delta^{18}O_v$ and $\delta^{18}O_p$ showed a significant decrease in the inland regions north of approximately 30°N, but unchanging in most regions south of 30°N. From the spatial distributions in October, both the ~~Ex~~ d_v and ~~Ex~~ d_p over the ocean or on land showed increases with varying degrees (Figs. 9e and 9f). The high-value regions of the ~~Ex~~ d_v were distributed along a line from the Arabian Peninsula, West Asia, the Tibetan Plateau, to Eastern Siberia, with the maximum value located in the Tibetan Plateau. The high-value region of ~~Ex~~ d_p was distributed from the Arabian Peninsula, West Asia, the Tibetan Plateau, to the Yunnan-Guizhou Plateau. With the weakening of the summer monsoon, the ~~Ex~~ d_v and ~~Ex~~ d_p were not significantly different in East Asia including the Dongting Lake Basin from those in the surrounding oceans.

Based on the vector interpolation of the Q field (Fig. 9a), the water vapor transport path was determined in October according to the method introduced in section 3.2.1 (indicated by the black arrow line in Fig. 9). This water vapor transport path originated from the western Pacific, passed through the South China Sea, flowed westward along the easterly jet located in the south of the West Pacific Subtropical High and of the anticyclonic circulation over the Jiangnan region in China, and finally entered the Dongting Lake Basin bypassing the southwest of the anticyclone. Although this water vapor path belonged to the latitudinal transport, the water vapor source originated from the low-latitude oceans of the western Pacific.

The corresponding Q, P, $\delta^{18}O_p$, $\delta^{18}O_v$, ~~Ex~~ d_v, and ~~Ex~~ d_p along the water vapor transport path were derived in October (Fig. 10). Under the stable atmospheric circulation conditions, the average water vapor flux steadily decreased from

681   approximately 299.0 kg m^{-1} s^{-1} in the source region to 168.0 kg m^{-1} s^{-1} along the water

682   vapor transport path, and further below 100.0 kg m^{-1} s^{-1}after entering the Dongting Lake

683   Basin (Fig. 10a). The *P* values changed gradually along the water vapor transport path,

684   decreasing from the initial approximately 145 mm to below 100 mm in the Dongting

685   Lake Basin, and further to 60.5 mm in the Changsha region (Fig. 10b). Both the $\delta^{18}O_v$

686   and $\delta^{18}O_p$ values showed slow decreases as the ranges within 2.0‰ and 1.0‰

687   respectively (Figs. 10c and 10d). The ~~Ex~~ d_v showed minor fluctuation, stabilizing at

688   approximately 16.8‰, while the corresponding ~~Ex~~ d_p remained around 8.6‰ before

689   entering the Dongting Lake Basin. Due to the replenishment from the surface

690   evaporation, the ~~Ex~~ d_p values increased to 11.6‰ after entering the Dongting Lake

691   Basin (Figs. 10e and 10f).

692
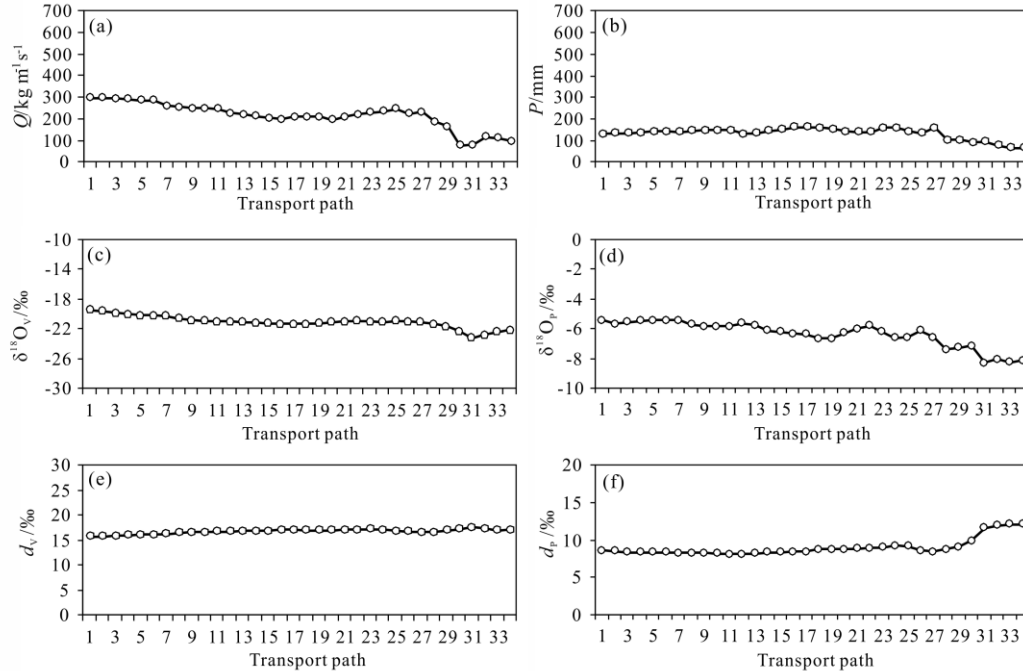
693   Fig. 10 Mean variations of *Q* (a), *P* (b), $\delta^{18}O_v$ (c), $\delta^{18}O_p$ (d), ~~Ex~~ d_v (e), and ~~Ex~~ d_p (f)

694   along the vapor transport path in October

695   **4. Discussion**

4.1 The Influences of the Seasonality in Water Vapor Sources on the Precipitation Isotopes.

The comparisons between the Q and $\delta^{18}O_p$ in the representative months indicated that there seems to be no obvious correspondence between these two factors: the months with low Q would exhibit either high or low $\delta^{18}O_p$, e.g. January and October, respectively (Figs. 3 and 9). Similarly, the months with high Q would exhibit either low or high $\delta^{18}O_p$, for example, June and April, respectively (Figs. 5 and 7). It has been found that regardless of the season, the precipitation in the Dongting Lake Basin mainly originated from warm and moist water vapor in low latitudes (Figs. 3, 5, 7, and 9). Therefore, whether the water vapor isotopes at the source regions and along the transport path influence the downstream isotopes of precipitation or water vapor? To reveal this causality, after considering the water vapor transport paths and the air mass properties of water vapor in the representative months, the water vapor regions corresponding to the Arabian Peninsula (40°E~56°E, 16°N~28°N), the Arabian Sea (56°E~74°E, 10°N~20°N), the Bay of Bengal (80°E~98°E, 8°N~18°N), and the western Pacific Ocean (120°E~160°E, 6°N~20°N), along with the inland regions of Dongting Lake Basin (110°E~114°E, 25°N~30°N) and East Asia monsoon region (110°E~135°E, 42°N~55°N) were labeled as Regions I, II, III, IV, V, and VI, respectively (Fig. 11). The average $\delta^{18}O$ and deuterium excessEx d of water vapor and precipitation for each representative region were calculated in January, April, June, and October, respectively. Since the seasonal variations in the $\delta^{18}O_v$ were similar to that in $\delta^{18}O_p$, Table 1 only provided the average $\delta^{18}O$ and deuterium excessEx d of water

718 vapor for each representative region.
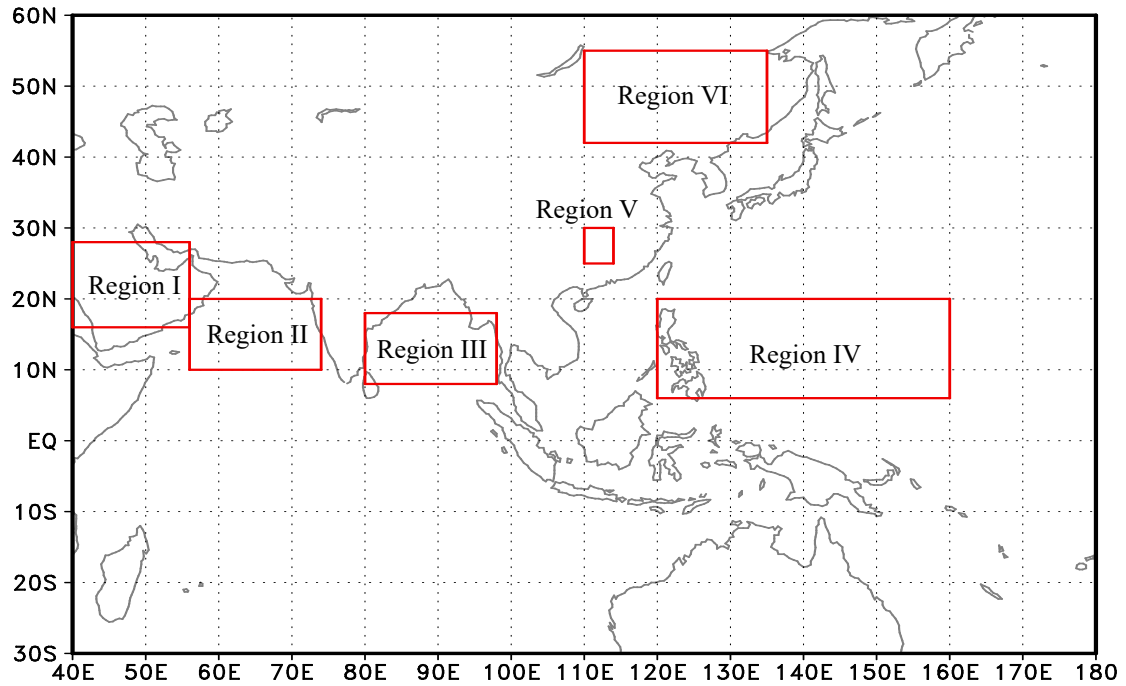
720 Fig. 11 Geographical distribution of representative regions

721 (Region I: Arabian Peninsula, Region II: Arabian Sea, Region III: Bay of Bengal,

722 Region IV: Western Pacific, Region V: Dongting Lake Basin, Region VI: Inland of the

723 East Asian monsoon region at middle and high latitudes)

724 Not only in Regions I to V located at mid to low latitudes but also in Region VI

725 located in the mid to high latitude inland regions, there was significant seasonality in

726 the average $\delta^{18}O_v$ and ~~Ex~~ d_v (Table 1). The seasonal ranges in the $\delta^{18}O_v$ (the differences

727 between the monthly maximum and minimum values) in these six representative

728 regions were 2.9‰, 3.3‰, 4.2‰, 5.1‰, 7.2‰, and 18.9‰, respectively, with the

729 largest seasonal range in $\delta^{18}O_v$ appeared in Region VI (Table 1). Except for Region VI,

730 the minimum values of the monthly $\delta^{18}O_v$ in other representative regions, all occurred

731 in October, while the maximum or second maximum values occurred in April. The

732 seasonal ranges in the ~~Ex~~ d_v in these six representative regions were 4.7‰, 5.4‰,

3.6‰, 3.8‰, 3.6‰, and 9.3‰, respectively, with the largest seasonal range in the ~~Ex~~ d_v

still in Region VI. Except for Region VI, the maximum values of monthly ~~Ex~~ d_v in

other representative regions mostly occurred in October, while the minimum or second

minimum values occurred in April or June (Table 1). These results indicated significant

differences in water vapor isotopes between Region VI and other oceanic or continental

representative regions, simultaneously, it can be found that oceanic water vapor had

varying degrees of impact on the isotopic composition of water vapor and precipitation

in Region VI and Region V, both located within the East Asian monsoon region, across

different seasons. With emphasis, the numeric comparisons above can also be used to

determine whether the major source of water vapor is oceanic or continental, especially

based on the judgment of excess deuterium values (i.e. ~~Ex~~ d_v), because the water vapor

coming from the Arabian Peninsula in winter (Fig. 3) had relatively high ~~Ex~~ d_v values

(Table 1, Region I), while the large amount of water vapor coming from the oceanic

representative regions in summer (Fig. 7) had very low ~~Ex~~ d_v values (Table 1, Region

III). These different sources of water vapor were ultimately reflected in their impact on

the isotopic composition of precipitation in the Dongting Lake Basin.

Table 1 Mean $\delta^{18}O_v$ and ~~Ex~~ d_v for representative regions in the representative months

Factors	Months	Region I	Region II	Region III	Region IV	Region V	Region VI
$\delta^{18}O_v$ /‰	January	−19.1	−17.4	−18.7	−17.2	−18.8	−40.9
	April	−16.2	−15.8	−17.8	−17.9	−14.9	−28.7
	June	−17.1	−14.5	−18.1	−21.9	−20.8	−22.0
	October	−19.2	−17.8	−22.0	−22.3	−22.1	−29.3
	January	18.5	18.5	17.2	14.4	15.2	23.2

~~Ex~~ d$_v$	April	16.9	17.5	17.0	13.9	13.6	15.6
	June	16.0	13.1	14.0	16.3	15.0	13.9
/‰	October	20.7	17.3	17.5	17.7	17.1	18.3

Furthermore, by comparing the water vapor isotopes in Region V with those in Region VI, it can be found that although both regions were all located in the East Asian monsoon region, there were differences in the seasonal variations of water vapor isotopes (Table 1; Fig. 11). For instance, the average $\delta^{18}O_v$ in Regions V and VI in all of the representative months were −19.2‰ and −30.2‰, respectively, with a difference of 11.1‰. Moreover, the average $\delta^{18}O_v$ of these two regions showed the largest differences with a value of 22.1‰ in January, which represented the peak of the winter monsoon, while in June which represented the peak of the summer monsoon, the difference was only 1.2‰. The water vapor isotopes in Region V were consistently enriched compared to those in Region VI. The average ~~Ex~~ d$_v$ in Regions V and VI in all of the representative months were 15.2‰ and 17.8‰, respectively, with a difference of −2.5‰, which was not too large. The difference was largest in January, reaching −8.0‰, while in June, the difference was only 1.14‰, indicating that the water vapor sources during the summer monsoon were similar in these two regions (Table 1).

The above results about the water stable isotope differences between the representative regions conform to the latitudinal and continental effects of water stable isotopes and follow the law of material migration, which states that the composition of water stable isotopes becomes more depleted with increasing latitude and water vapor transport from high to low value regions (Feng et al., 2009; Zhang et al., 2012; Zhang et al., 2016). With emphasis, for the water vapor source of precipitation in the Dongting

Lake Basin, the oceanic representative regions located at low latitudes may not

necessarily be the initial water vapor source regions, and the relationship between

upstream and downstream regions may not entirely be point-to-point, as there were

continuous water recycling and rainout processes along the water vapor transport path

(Pokam et al., 2012; Risi et al., 2013; Christner et al., 2018).

However, through the comparisons above, it can be observed that the influences

of upstream regions on the water vapor amount and water vapor isotopes in downstream

regions during water vapor transport were significant. For instance, two distinct water

vapor transport paths were identified in April (Fig. 5), thus it is crucial to assess which

path exerted a more significant influence on the isotopic composition of precipitation

in the Dongting Lake Basin, with priority given to the path whose air parcel isotopic

signature closely matches the precipitation isotopes in the basin before entry. According

to this principle and referring to Table 1, we observed that in April, the average $\delta^{18}O_v$

and Ex d_v values of the Dongting Lake Basin (i.e. Region V) were $-14.9‰$ and $13.6‰$,

respectively. Moreover, before entering the Dongting Lake Basin, the $\delta^{18}O_v$ and Ex d_v

values of the air parcel on the first water vapor transport path—that is, Path I, were

$-14.9‰$ and $14.3‰$, respectively (Figs. 6c and 6e). For the second transport path—that

is, Path II, these values were $-14.9‰$ and $13.5‰$, respectively (Figs. 6c and 6e).

Besides, it is worth noting the complexity of isotopic variations along the water vapor

transport paths, where numerous processes can influence the isotopic composition of

air masses over long distances, and such variations are a continuous process with

cumulative effects. These processes include rainout, evaporation recharge, mixing with

other air vapor masses, and changes in temperature and humidity, all of which contribute to the cumulative isotopic variations along the transport paths. Therefore, the primary criterion for determining the relative impact of these paths is the water vapor flux Q. As shown in Fig. 6a, the water vapor flux Q associated with Path II is significantly higher than that of Path I before reaching the Dongting Lake Basin. This larger flux indicated that Path II contributed more water vapor to the Dongting Lake Basin, thereby having a more substantial influence on the local precipitation isotopes. Clearly, the oceanic air mass with low deuterium excess had a relatively more significant impact on the precipitation isotopes in April in the Dongting Lake Basin region.

In this study, we focus on the climatological mean state of water vapor transport and its influence on precipitation in the Dongting Lake Basin over four representative months (January, April, June, and October, which representing winter, spring, summer, and autumn, respectively) from 1979 to 2017. Our analysis is based on the monthly average values of vertical integral water vapor flux Q, precipitation amount P, and isotopic compositions of water vapor and precipitation. This approach reflects the general characteristics of water vapor transport paths and their influence on precipitation for each month, rather than focusing on individual precipitation events. The magnitude of water vapor flux Q is directly related to precipitation amounts P, and thus, our analysis does not require differentiation between precipitating and non-precipitating days. For example, low values of water vapor flux Q in January and October correspond to low precipitation amounts, indicating that the overall transport

814 conditions are less conducive to precipitation.

4.2 Isotopic Properties of Air Masses

According to the definition of meteorology, air mass refers to a large-scale body of air over land or sea with relatively uniform horizontal physical properties such as temperature, humidity, and atmospheric stability. The horizontal extent of an air mass ranges from 10^2 km to 10^3 km, and the vertical extent ranges from 10^0 km to 10^1 km, while within the same air mass, there is little variation in temperature gradients, atmospheric vertical stability, and weather phenomena (Zhou et al., 1997). Under large-scale and relatively uniform underlying surfaces and stable atmospheric circulation conditions, water vapor and its transport belong to the characteristics of air masses or have the properties of the air mass origin regions (Dettinger, 2013; Lavers et al., 2013). Considering the sources and sinks of water vapor, the spatial distribution of water vapor isotopes is relatively similar within an air mass. In oceanic air masses, the isotopic values of water vapor are relatively higher compared to those in continental air masses, while the deuterium excess of water vapor is typically lower. Conversely, in continental air masses, water vapor isotopes are relatively depleted but the d-excess can be higherIn oceanic air masses, water vapor isotopes are relatively enriched, while deuterium excess of water vapor is relatively more negative, while in continental air masses, water vapor isotopes are relatively depleted, while deuterium excess of water vapor is relatively more negative (Rozanski et al., 1993; Araguás-Araguás et al., 1998).

With the seasonal variation in the position of the sun's orbit, the atmospheric circulation conditions undergo seasonal variations and thus lead to the seasonality of

the air masses properties (Qian et al., 2009; Parding et al., 2016). The abundance of

water vapor isotopes at a fixed location varies due to variations in circulation conditions

(Lacour et al., 2018; Dee et al., 2018; Gou et al., 2022). In this study, the isotopic

compositions of water vapor in oceanic Regions II and IV at low latitudes and in inland

Region VI at high latitudes exhibited significant seasonal variations due to interactions

between tropical continental air masses (located in southern West Asia) and tropical

oceanic air masses, between tropical oceanic air masses and equatorial air masses, and

between temperate continental air masses and temperate oceanic air masses,

respectively (Table 1; Fig. 11). In the process of seasonal changes, as air masses move

out of their source regions, their physical and weather characteristics also change with

the variations in underlying surface properties and large-scale vertical motion

conditions.

East Asia is primarily controlled by the "modified"modificatory air masses, which

were commonly used to describe the properties (e.g., temperature, pressure, and

humidity) of air masses that have changed as they move through different regions (Ding,

1990; Chang et al., 2012). For instance, as an air mass moves from a warm and moist

region to a cooler and drier region, its temperature and humidity can change

significantly. Similarly, interactions with topography and varying surface conditions

can lead to modifications in the air mass properties. This concept is particularly relevant

in regions like East Asia, where air masses can be significantly altered as they pass

through different climatic zones. Whether cold and dry air masses moving southward

or warm and moist air masses moving northward, the isotopic composition of water

vapor in the "modified" ~~modificatory~~ air mass continues to become more negative, while the deuterium excess of water vapor continues to become more positive than the original air mass, following the variation rule of stable isotope and deuterium excess during water vapor transport (Vasil'chuk, 2014; Zhou et al., 2019; Xu et al., 2019; Jackisch et al., 2022). In this study, interactions between "modified" ~~modificatory~~ oceanic air mass and "modified" ~~modificatory~~ continental air mass result in the water vapor isotope in Region V that differed from oceanic air masses and continental air masses (Table 1; Fig. 11). In summary, based on the comparison of stable isotopes of water vapor and precipitation in different seasons and representative regions presented in this study, it can be observed that, as an integral component of the climate system, air masses in various regions not only exhibit differences in thermodynamic, dynamic, hydrous, and static properties, but are also influenced by interactions between air masses, the underlying surface, and the intensity of convection, among others.

4.3 The Difference Between Water Vapor Field and Wind Field

The water vapor flux Q reflects the direction and magnitude of water vapor transport in the atmosphere, while wind V reflects the direction and magnitude of the movement of air particles in the atmosphere (Feng et al., 2009; Zhang et al., 2012; Zhang et al., 2016). There are both differences and connections between the two factors. Water vapor is transported by wind, and the wind carries water vapor from one place to another, and the directions of water vapor and wind may be consistent, inconsistent, or even opposite. In the East Asian monsoon region, the prevailing wind direction during the summer monsoon period is generally consistent with the average water vapor

880   transport direction, both being southwest or southeast direction (Barker, et al., 2015;

881   Wu et al., 2015; Tang et al., 2015). In this study, the water vapor transport path was

882   consistent with the prevailing wind direction in June (Figs. 1a and 9). However, during

883   the winter monsoon period, the prevailing wind direction may not be consistent with

884   the average transport direction of water vapor—that is, the prevailing wind direction in

885   January was northwest or northeast direction, while the average transport direction of

886   water vapor in this period was southwest or southeast direction (Figs. 1a and 3).

887   Previous studies have shown that the most common weather systems and most

888   precipitation events in the East Asian monsoon region are caused by cold fronts

889   resulting from the interaction of warm and cold air masses (Chen et al., 2020).

890   According to classical meteorological theory (Zhou et al., 1997), in a cold front system,

891   there appears the wind from the southwest direction blows ahead of the front, and a

892   northwest wind blows behind the front as shown in the schematic diagram in Fig. 12a.

893   Warm and moist air from low latitudes lifts along the front and leads to rainfall, while

894   cold and dry air from high latitudes moves southward beneath the front and lifts the

895   warm and moist air. At different heights and positions, the directions of air particle

896   movement and water vapor transport are different. For example, at point A located

897   above the warm and moist air side of the cold front surface, both air particles and water

898   vapor are transported by southwest wind. At point C located below the cold, dry air side

899   of the cold front surface, both air particles and water vapor are transported by northwest

900   wind. However, at point B located within the front zone, the wind direction and speed

901   are uncertain (Fig. 12b). Specifically, this front zone marked the transition from a warm

902 air mass to a cold one, or vice versa, where meteorological factors have undergone rapid

903 changes. Mixing between cold and warm advected air could occur within this zone,

904 manifesting as a shear zone in wind fields, or as alternating southerly and northerly

905 winds. Therefore, the dominant wind directions may not always align with the average

906 water vapor transport direction, especially in frontal weather systems that dominate

907 precipitation in the East Asian monsoon region. Our study focuses on the Q field (the

908 vertical integral of water vapor flux) to determine water vapor transport paths, which

909 directly reflect the direction and magnitude of water vapor transport in the atmosphere.

910 This method is distinct from particle dispersion models or back-trajectory models,

911 which are based on the movement of air particles (wind direction). As discussed earlier,

912 water vapor is transported by wind, but the directions of water vapor transport and wind

913 may not always align, especially in complex weather systems such as cold fronts.

914
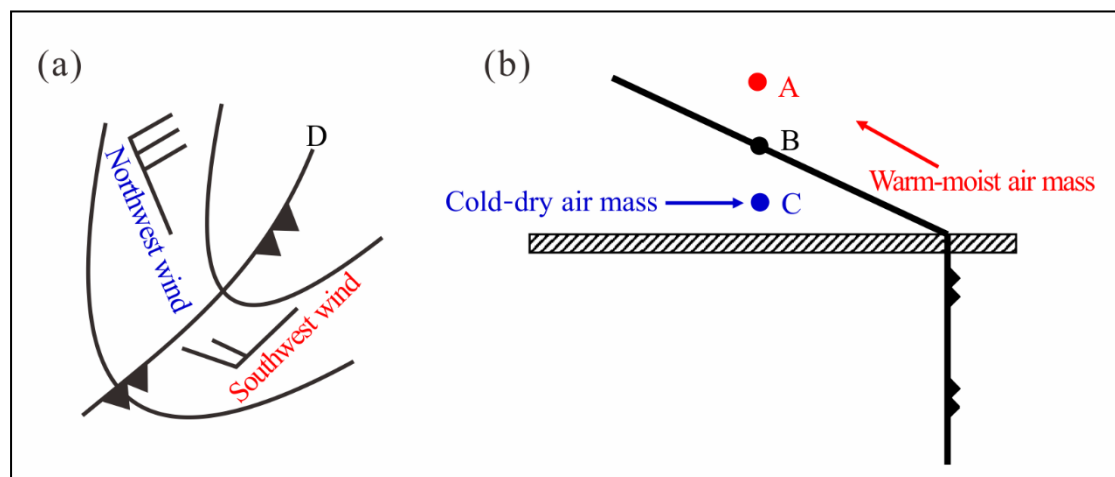
915 Fig. 12 Schematic diagram of a cold front system in East Asia (based on Zhou et al.,

916 1997).

917 **4. Conclusion**

918   Our findings revealed significant influences of water vapor source and transport

on precipitation isotopes in Dongting Lake Basin. Specifically, in January, water vapor contributing to the Dongting precipitation originated near the Arabian Peninsula and was driven by the southern branch of the westerly stream jet on the southern side of the Tibetan Plateau, water vapor transported along the southern side of the Tibetan Plateau, passed through southwestern China via the northern part of the Indian Peninsula, and reached the Dongting Lake Basin. In April, two distinct water vapor transport paths contributed to the Dongting precipitation, the first followed a trajectory similar to the average water vapor transport path in January, albeit shifted slightly northward by one degree of latitude. The second transport path, driven by the weak Western Pacific subtropical high, guided warm and moist water vapor from the low latitudes of the Western Pacific along the outer edge of the subtropical high, passing through the South China Sea and the Indochinese Peninsula and finally reached into the Dongting Lake Basin. In June, the precipitation in the Dongting Lake Basin was influenced by a water vapor transport path originating from the northern branch of the South Indian Ocean subtropical high, crossed the equator, and transported through the Somali Sea, the Arabian Sea, the Indian Peninsula, the Bay of Bengal, the Indochinese Peninsula, and entered the southwestern region of China, finally reaching the Dongting Lake Basin. In October, the average water vapor transport path originated from the western Pacific, passed through the South China Sea, flowed westward along the easterly jet located in the south of the West Pacific Subtropical High and of the anticyclonic circulation over the Jiangnan region in China, and finally entered the Dongting Lake Basin bypassing the southwest of the anticyclone. Although this water vapor path belonged to the

latitudinal transport, the water vapor source originated from the low-latitude oceans of the western Pacific. In these four months representing different seasons, variations in the $\delta^{18}O$ and deuterium excess of precipitation and water vapor along these water vapor transport paths show some agreement with Rayleigh fractionation and water balance principles. This highlights the complex transport paths and processes that influence isotopic variations in precipitation in the Dongting Lake Basin~~In these four months that representing different seasons, variations in the $\delta^{18}O$ and Ex_d of precipitation and water vapor along these water vapor transport paths adhered to principles of Rayleigh fractionation and water balance principles, underscoring the complex transport paths and processes that influence isotopic variations in precipitation in the Dongting Lake Basin~~. However, the prevailing wind direction may not be consistent with the average transport direction of water vapor, especially during the winter monsoon, which can be explained by the water vapor field and wind field in frontal weather systems that dominate precipitation in the East Asian monsoon region.

Overall, the approach utilized in this study is grounded in fundamental meteorological theories, specifically involving water vapor diagnosis and calculations (including source regions, transport paths, and transport quantities), this analytical method is robust and has a clear physical basis. The scientific question addressed by this study is not centered on the spatial and temporal variations of water isotopes, but rather on how the seasonal variations in regional precipitation and precipitation isotopes respond to the seasonal variations in water vapor sources and transport. A potential direction for future research could be to investigate the intra-seasonal variations in

composite differences across various factors, rather than focusing on inter-seasonal comparisons.

Competing interests

The authors declare that they have no known competing financial interests or personal relationships that could have appeared to influence the work reported in this paper.

Acknowledgments

This study was supported by the Natural Science Foundation of Hunan Province, China (No. 2023JJ40445) the National Natural Science Foundation of China (No. 42101130), and the Aid Program for Science and Technology Innovative Research Team in Higher Educational Institutions of Hunan Province (0531120-4944). We are grateful to the graduate students who laboriously sampled water samples without interruption and tested water stable isotopes for 13 years.

Data availability statement.

The global atmospheric reanalysis data and water stable isotope simulation data are downloaded from the ECMWF 5th generation atmospheric reanalysis data (ERA5, https://cds.climate.copernicus.eu/) and the second-generation isoGSM2 dataset (https://datadryad.org/stash/dataset/doi:10.6078/D1MM6B), respectively. The stable isotopic data of precipitation and meteorological data at the Changsha station are accessible by emailing the corresponding author (zxp@hunnu.edu.cn) with a reasonable request.

Author contribution

XX: Methodology, Software, Writing- Original draft preparation, Reviewing and

Editing. XPZ: Supervisor, Guide, Data curation, Methodology, Software, Writing-Original draft preparation, Reviewing and Editing. ZYX: Methodology, Writing-Original draft preparation. ZLL, DZW, CCZ, ZGR, XGH, and HDG: Methodology, Reviewing and Editing. All authors made substantial contributions to the discussion of content.

References:

Albergel, C., Dutra, E., Munier, S., Calvet, J. C., Munoz-Sabater, J., de Rosnay, P., & Balsamo, G. (2018). ERA-5 and ERA-Interim driven ISBA land surface model simulations: which one performs better?. Hydrology and Earth System Sciences, 22(6), 3515-3532.

Araguás-Araguás, L., Froehlich, K., & Rozanski, K. (1998). Stable isotope composition of precipitation over southeast Asia. Journal of Geophysical Research: Atmospheres, 103(D22), 28721-28742.

Baker, A. J., Sodemann, H., Baldini, J. U., Breitenbach, S. F., Johnson, K. R., van Hunen, J., & Zhang, P. (2015). Seasonality of westerly moisture transport in the East Asian summer monsoon and its implications for interpreting precipitation $\delta^{18}O$. Journal of Geophysical Research: Atmospheres, 120(12), 5850-5862.

Bong, H., Cauquoin, A., Okazaki, A., Chang, E. C., Werner, M., Wei, Z., ... & Yoshimura, K. (2024). Process-Based Intercomparison of Water Isotope-Enabled Models and Reanalysis Nudging Effects. Journal of Geophysical Research: Atmospheres, 129(1), 1-28.

Chang, C. P., Lei, Y., Sui, C. H., Lin, X., & Ren, F. (2012). Tropical cyclone and extreme rainfall trends in East Asian summer monsoon since mid - 20th century. Geophysical Research Letters, 39(18), 1-7.

Chen, X., Zhang, X. Z., Zhang X. P., & Long X. (2020). Long-term Variation of Regional Extreme Precipitation in jiangnan Area and Its Possible Cause. Resources and Environment in The Yangtze Basin, 29(08),1757-1767.

Chiang, J. C., Herman, M. J., Yoshimura, K., & Fung, I. Y. (2020). Enriched East Asian oxygen isotope of precipitation indicates reduced summer seasonality in regional climate and westerlies. Proceedings of the National Academy of Sciences, 117(26), 14745-14750.

Christner, E., Aemisegger, F., Pfahl, S., Werner, M., Cauquoin, A., Schneider, M., ... & Schädler, G. (2018). The climatological impacts of continental surface evaporation, rainout, and subcloud processes on δD of water vapor and precipitation in Europe. Journal of Geophysical Research: Atmospheres, 123(8), 4390-4409.

Albergel, C., Dutra, E., Munier, S., Calvet, J. C., Munoz-Sabater, J., de Rosnay, P., and Balsamo, G.: ERA-5 and ERA-Interim driven ISBA land surface model simulations: which one performs better?, Hydrol. Earth Syst. Sci., 22, 3515-3532, https://doi.org/10.5194/hess-22-3515-2018, 2018.

Araguás-Araguás, L., Froehlich, K., and Rozanski, K.: Stable isotope composition of precipitation over southeast Asia, J. Geophys. Res.-Atmos., 103, 28721-28742, https://doi.org/10.1029/98JD02582, 1998.

Baker, A. J., Sodemann, H., Baldini, J. U., Breitenbach, S. F., Johnson, K. R., van Hunen, J., and Zhang, P.: Seasonality of westerly moisture transport in the East Asian summer monsoon and its implications for interpreting precipitation $\delta^{18}O$, J. Geophys. Res.-Atmos., 120, 5850-5862, https://doi.org/10.1002/2014JD022919, 2015.

Bong, H., Cauquoin, A., Okazaki, A., Chang, E. C., Werner, M., Wei, Z., and Yoshimura, K.: Process-Based Intercomparison of Water Isotope-Enabled Models and Reanalysis Nudging Effects, J. Geophys. Res.-Atmos., 129, 1-28, https://doi.org/10.1029/2023JD038719, 2024.

Chang, C. P., Lei, Y., Sui, C. H., Lin, X., and Ren, F.: Tropical cyclone and extreme rainfall trends in East Asian summer monsoon since mid-20th century, Geophys. Res. Lett., 39, 1-7, https://doi.org/10.1029/2012GL052945, 2012.

Chen, X., Zhang, X. Z., Zhang, X. P., and Long, X.: Long-term Variation of Regional Extreme Precipitation in Jiangnan Area and its Possible Cause (in Chinese with English abstract), Resour. Environ. Yangtze Basin, 29, 1757-1767, https://doi.org/10.11870/cjlyzyyhj202008008, 2020.

Chiang, J. C., Herman, M. J., Yoshimura, K., and Fung, I. Y.: Enriched East Asian oxygen isotope of precipitation indicates reduced summer seasonality in regional climate and westerlies, Proc. Natl. Acad. Sci. USA, 117, 14745-14750, https://doi.org/10.1073/pnas.1922602117, 2020.

Christner, E., Aemisegger, F., Pfahl, S., Werner, M., Cauquoin, A., Schneider, M., and Schädler, G.: The climatological impacts of continental surface evaporation,

rainout, and subcloud processes on δD of water vapor and precipitation in Europe, J. Geophys. Res.-Atmos., 123, 4390-4409, https://doi.org/10.1002/2017JD027260, 2018.

Dahinden, F., Aemisegger, F., Wernli, H., Schneider, M., Diekmann, C. J., Ertl, B., and Pfahl, S.: Disentangling different moisture transport pathways over the eastern subtropical North Atlantic using multi-platform isotope observations and high-resolution numerical modeling, Atmos. Chem. Phys., 21, 16319-16347, https://doi.org/10.5194/acp-21-16319-2021, 2021.

Dee, S. G., Nusbaumer, J., Bailey, A., Russell, J. M., Lee, J. E., Konecky, B., and Noone, D. C.: Tracking the strength of the Walker circulation with stable isotopes in water vapor, J. Geophys. Res.-Atmos., 123, 7254-7270, https://doi.org/10.1029/2017JD027915, 2018.

Deng, H., Wang, Q., Zhao, Y., Zhai, J., Zhu, Y., Gui, Y., and Liu, K.: Effect of water vapor transport and budget on precipitation in the Yangtze–Huang–Huai–Hai River Basin, J. Hydrol. Reg. Stud., 53, 101787, https://doi.org/10.1016/j.ejrh.2024.101787, 2024.

Dettinger, M. D.: Atmospheric rivers as drought busters on the US West Coast, J. Hydrometeorol., 14, 1721-1732, https://doi.org/10.1175/JHM-D-13-02.1, 2013.

Dahinden, F., Aemisegger, F., Wernli, H., Schneider, M., Diekmann, C. J., Ertl, B., ... & Pfahl, S. (2021). Disentangling different moisture transport pathways over the eastern subtropical North Atlantic using multi-platform isotope observations

and high-resolution numerical modelling. Atmospheric Chemistry and Physics, 21(21), 16319-16347.

Dee, S. G., Nusbaumer, J., Bailey, A., Russell, J. M., Lee, J. E., Konecky, B., ... & Noone, D. C. (2018). Tracking the strength of the Walker circulation with stable isotopes in water vapor. Journal of Geophysical Research: Atmospheres, 123(14), 7254-7270.

Deng, H., Wang, Q., Zhao, Y., Zhai, J., Zhu, Y., Gui, Y., ... & Liu, K. (2024). Effect of water vapor transport and budget on precipitation in the Yangtze Huang Huai Hai River Basin. Journal of Hydrology: Regional Studies, 53, 101787.

Dettinger, M. D. (2013). Atmospheric rivers as drought busters on the US West Coast. Journal of Hydrometeorology, 14(6), 1721-1732.Ding, Y., 1990: Build-up, air mass transformation and propagation of Siberian high and its relations to cold surge in East Asia. Meteorology and Atmospheric Physics, 44, 281-292.

Esquivel-Hernández, G., Mosquera, G. M., Sánchez-Murillo, R., Quesada-Román, A., Birkel, C., Crespo, P., and Boll, J.: Moisture transport and seasonal variations in the stable isotopic composition of rainfall in Central American and Andean Páramo during El Niño conditions (2015–2016), Hydrol. Process., 33, 1802-1817, https://doi.org/10.1002/hyp.13438, 2019.

Feng, X., Faiia, A. M., and Posmentier, E. S.: Seasonality of isotopes in precipitation: A global perspective, J. Geophys. Res.-Atmos., 114, 1-13, https://doi.org/10.1029/2008JD011279, 2009.

Gimeno, L., Vázquez, M., Eiras-Barca, J., Sorí, R., Stojanovic, M., Algarra, I., and Dominguez, F.: Recent progress on the sources of continental precipitation as revealed by moisture transport analysis, Earth-Sci. Rev., 201, 103070, https://doi.org/10.1016/j.earscirev.2019.103070, 2020.

Gou, J., Qu, S., Guan, H., Shi, P., Su, Z., Lin, Z., and Zhu, J.: Relationship between precipitation isotopic compositions and synoptic atmospheric circulation patterns in the lower reach of the Yangtze River, J. Hydrol., 605, 127289, https://doi.org/10.1016/j.jhydrol.2021.127289, 2022.

Guo, L., Van Der Ent, R. J., Klingaman, N. P., Demory, M. E., Vidale, P. L., Turner, A. G., and Chevuturi, A.: Moisture sources for East Asian precipitation: Mean seasonal cycle and interannual variability, J. Hydrometeorol., 20, 657-672, https://doi.org/10.1175/JHM-D-18-0188.1, 2019.

He, H., Cao, R., Wu, Z. Y., Li, Y., Yin, H., and Yuan, F.: Diagnosing anomalous characteristics of atmospheric water cycle structure during seasonal-scale drought events: A case study in middle and lower reaches of Yangtze River, Water Sci. Eng., 15, 103-113, https://doi.org/10.1016/j.wse.2022.01.001, 2022.

Hoffmann, L., Günther, G., Li, D., Stein, O., Wu, X., Griessbach, S., and Wright, J. S.: From ERA-Interim to ERA5: the considerable impact of ECMWF's next-generation reanalysis on Lagrangian transport simulations, Atmos. Chem. Phys., 19, 3097-3124, https://doi.org/10.5194/acp-19-3097-2019, 2019.

Hu, Q., Jiang, D., Lang, X., and Yao, S.: Moisture sources of summer precipitation over eastern China during 1979–2009: A Lagrangian transient simulation, Int. J. Climatol., 41, 1162-1178, https://doi.org/10.1002/joc.6781, 2021.

Huang, H., and Li, L.: A Synchronous Variation Process of Tibetan Plateau Vortex and Southwest Vortex (in Chinese with English abstract), J. Appl. Meteorol. Sci., 34, 451-462, https://doi.org/10.11898/1001-7313.20230406, 2023.

Jackisch, D., Yeo, B. X., Switzer, A. D., He, S., Cantarero, D. L. M., Siringan, F. P., and Goodkin, N. F.: Precipitation stable isotopic signatures of tropical cyclones in Metropolitan Manila, Philippines, show significant negative isotopic excursions, Nat. Hazards Earth Syst. Sci., 22, 213-226, https://doi.org/10.5194/nhess-22-213-2022, 2022.

Kathayat, G., Sinha, A., Tanoue, M., Yoshimura, K., Li, H., Zhang, H., and Cheng, H.: Interannual oxygen isotope variability in Indian summer monsoon precipitation reflects changes in moisture sources, Commun. Earth Environ., 2, 1-10, https://doi.org/10.1038/s43247-021-00165-z, 2021.

Lacour, J. L., Risi, C., Worden, J., Clerbaux, C., and Coheur, P. F.: Importance of depth and intensity of convection on the isotopic composition of water vapor as seen from IASI and TES δD observations, Earth Planet. Sci. Lett., 481, 387-394, https://doi.org/10.1016/j.epsl.2017.10.048, 2018.

Lai, X., Wang, Q., Huangfu, J., Jiang, X., Wang, L., Chen, W., and Tang, Y.: Progress in Climatological Research on the Southwest China Vortex (in Chinese with

English abstract), Chinese J. Atmos. Sci., 47, 1983-2000, https://doi.org/10.3878/j.issn.1006-9895.2304.23021, 2023.

Lavers, D. A., Allan, R. P., Villarini, G., Lloyd-Hughes, B., Brayshaw, D. J., and Wade, A. J.: Future changes in atmospheric rivers and their implications for winter flooding in Britain, Environ. Res. Lett., 8, 034010, https://doi.org/10.1088/1748-9326/8/3/034010, 2013.

Lekshmy, P. R., Midhun, M., and Ramesh, R.: Role of moisture transport from Western Pacific region on water vapor isotopes over the Bay of Bengal, Atmos. Res., 265, 105895, https://doi.org/10.1016/j.atmosres.2021.105895, 2022.

Liu, J., Song, X., Fu, G., Liu, X., Zhang, Y., and Han, D.: Precipitation isotope characteristics and climatic controls at a continental and an island site in Northeast Asia, Clim. Res., 49, 29-44, https://doi.org/10.3354/cr01013, 2011. Esquivel-Hernández, G., Mosquera, G. M., Sánchez-Murillo, R., Quesada-Román, A., Birkel, C., Crespo, P., ... & Boll, J. (2019). Moisture transport and seasonal variations in the stable isotopic composition of rainfall in Central American and Andean Páramo during El Niño conditions (2015–2016). Hydrological Processes, 33(13), 1802-1817.

Feng, X., Faiia, A. M., & Posmentier, E. S. (2009). Seasonality of isotopes in precipitation: A global perspective. Journal of Geophysical Research: Atmospheres, 114(D8), 1-13.

Gimeno, L., Vázquez, M., Eiras-Barca, J., Sorí, R., Stojanovic, M., Algarra, I., ... & Dominguez, F. (2020). Recent progress on the sources of continental precipitation as revealed by moisture transport analysis. Earth-Science Reviews, 201, 103070.

Gou, J., Qu, S., Guan, H., Shi, P., Su, Z., Lin, Z., ... & Zhu, J. (2022). Relationship between precipitation isotopic compositions and synoptic atmospheric circulation patterns in the lower reach of the Yangtze River. Journal of Hydrology, 605, 127289, 1-15.

Guo, L., Van Der Ent, R. J., Klingaman, N. P., Demory, M. E., Vidale, P. L., Turner, A. G., ... & Chevuturi, A. (2019). Moisture sources for East Asian precipitation: Mean seasonal cycle and interannual variability. Journal of Hydrometeorology, 20(4), 657-672.

He, H., Cao, R., Wu, Z. Y., Li, Y., Yin, H., & Yuan, F. (2022). Diagnosing anomalous characteristics of atmospheric water cycle structure during seasonal-scale drought events: A case study in middle and lower reaches of Yangtze River. Water Science and Engineering, 15(2), 103-113.

Hoffmann, L., Günther, G., Li, D., Stein, O., Wu, X., Griessbach, S., ... & Wright, J. S. (2019). From ERA-Interim to ERA5: the considerable impact of ECMWF's next-generation reanalysis on Lagrangian transport simulations. Atmospheric Chemistry and Physics, 19(5), 3097-3124.

Hu, Q., Jiang, D., Lang, X., & Yao, S. (2021). Moisture sources of summer precipitation over eastern China during 1979-2009: A Lagrangian transient simulation. International Journal of Climatology, 41(2), 1162-1178.

Huang, H., & Li, L. (2023). A Synchronous Variation Process of Tibetan Plateau Vortex and Southwest Vortex (in Chinese with English abstract). Journal of Applied Meteorological Science, 34(4), 451-462.

Jackisch, D., Yeo, B. X., Switzer, A. D., He, S., Cantarero, D. L. M., Siringan, F. P., & Goodkin, N. F. (2022). Precipitation stable isotopic signatures of tropical cyclones in Metropolitan Manila, Philippines, show significant negative isotopic excursions. Natural Hazards and Earth System Sciences, 22(1), 213-226.

Kathayat, G., Sinha, A., Tanoue, M., Yoshimura, K., Li, H., Zhang, H., & Cheng, H. (2021). Interannual oxygen isotope variability in Indian summer monsoon precipitation reflects changes in moisture sources. Communications Earth & Environment, 2(1), 1-10.

Lacour, J. L., Risi, C., Worden, J., Clerbaux, C., & Coheur, P. F. (2018). Importance of depth and intensity of convection on the isotopic composition of water vapor as seen from IASI and TES δD observations. Earth and Planetary Science Letters, 481, 387-394.

Lai, X., Wang, Q., Huangfu, J., Jiang, X., Wang, L., Chen, W., ... & Tang, Yu. (2023). Progress in Climatological Research on the Southwest China Vortex (in Chinese with English abstract). Chinese Journal of Atmospheric Sciences, 47(6), 1983-2000.

Lavers, D. A., Allan, R. P., Villarini, G., Lloyd-Hughes, B., Brayshaw, D. J., & Wade, A. J. (2013). Future changes in atmospheric rivers and their implications for winter flooding in Britain. Environmental Research Letters, 8(3), 034010, 1-8.

Lekshmy, P. R., Midhun, M., & Ramesh, R. (2022). Role of moisture transport from Western Pacific region on water vapor isotopes over the Bay of Bengal. Atmospheric Research, 265, 105895.

Liu, J., Song, X., Fu, G., Liu, X., Zhang, Y., & Han, D. (2011). Precipitation isotope characteristics and climatic controls at a continental and an island site in Northeast Asia. Climate Research, 49(1), 29-44.

Liu, Z., Zhang, X., Xiao, Z., He, X., Rao, Z., and Guan, H.: The relations between summer droughts/floods and oxygen isotope composition of precipitation in the Dongting Lake basin, Int. J. Climatol., 43, 3590-3604, https://doi.org/10.1002/joc.8047, 2023.

Nie, Y., and Sun, J.: Moisture sources and transport for extreme precipitation over Henan in July 2021, Geophys. Res. Lett., 49, 1-10, https://doi.org/10.1029/2021GL097446, 2022.

Parding, K., Olseth, J. A., Liepert, B. G., and Dagestad, K. F.: Influence of atmospheric circulation patterns on local cloud and solar variability in Bergen, Norway, Theor. Appl. Climatol., 125, 625-639, https://doi.org/10.1007/s00704-015-1517-8, 2016.

Payne, A. E., Demory, M. E., Leung, L. R., Ramos, A. M., Shields, C. A., Rutz, J. J., and Ralph, F. M.: Responses and impacts of atmospheric rivers to climate change, Nat. Rev. Earth Environ., 1, 143-157, https://doi.org/10.1038/s43017-020-0030-5, 2020.

Pérez-Alarcón, A., Fernández-Alvarez, J. C., Sorí, R., Nieto, R., and Gimeno, L.: Moisture source identification for precipitation associated with tropical cyclone

development over the Indian Ocean: a Lagrangian approach, Clim. Dyn., 60, 2735-2758, https://doi.org/10.1007/s00382-022-06429-4, 2023.

Pokam, W. M., Djiotang, L. A. T., and Mkankam, F. K.: Atmospheric water vapor transport and recycling in Equatorial Central Africa through NCEP/NCAR reanalysis data, Clim. Dyn., 38, 1715-1729, https://doi.org/10.1007/s00382-011-1242-7, 2012.

Pranindita, A., Wang-Erlandsson, L., Fetzer, I., and Teuling, A. J.: Moisture recycling and the potential role of forests as moisture source during European heatwaves, Clim. Dyn., 58, 609-624, https://doi.org/10.1007/s00382-021-05921-7, 2022.

Qian, L., Solomon, S. C., and Kane, T. J.: Seasonal variation of thermospheric density and composition, J. Geophys. Res.-Space Phys., 114, 1-15, https://doi.org/10.1029/2008JA013643, 2009.

Ralph, F. M., Dettinger, M. D., Cairns, M. M., Galarneau, T. J., and Eylander, J.: Defining "atmospheric river": How the Glossary of Meteorology helped resolve a debate, Bull. Am. Meteorol. Soc., 99, 837-839, https://doi.org/10.1175/BAMS-D-17-0157.1, 2018.

Risi, C., Bony, S., Vimeux, F., Frankenberg, C., Noone, D., and Worden, J.: Understanding the Sahelian water budget through the isotopic composition of water vapor and precipitation, J. Geophys. Res.-Atmos., 115, 1-23, https://doi.org/10.1029/2010JD014690, 2010.

Risi, C., Noone, D., Frankenberg, C., and Worden, J.: Role of continental recycling in intraseasonal variations of continental moisture as deduced from model

simulations and water vapor isotopic measurements, Water Resour. Res., 49, 4136-4156, https://doi.org/10.1002/wrcr.20312, 2013.

Rozanski, K., Araguás-Araguás, L., and Gonfiantini, R.: Isotopic patterns in modern global precipitation, Climate change in continental isotopic records, 78, 1-36, https://doi.org/10.1029/GM078p0001, 1993.

Sengupta, S., and Sarkar, A.: Stable isotope evidence of dual (Arabian Sea and Bay of Bengal) vapour sources in monsoonal precipitation over north India, Earth Planet. Sci. Lett., 250, 511-521, https://doi.org/10.1016/j.epsl.2006.08.011, 2006.

Shi, X., Risi, C., Li, L., Wang, X., Pu, T., Zhang, G., and Kong, Y.: What controls the skill of general circulation models to simulate the seasonal cycle in water isotopic composition in the Tibetan Plateau region?, J. Geophys. Res.-Atmos., 127, e2022JD037048, https://doi.org/10.1029/2022JD037048, 2022.

Shi, Y., Jin, Z., Wu, A., Li, G., and Li, F.: Stable isotopic characteristics of precipitation related to the environmental controlling factors in Ningbo, East China, Environ. Sci. Pollut. Res., 28, 10696-10706, https://doi.org/10.1007/s11356-020-11332-8, 2021.

Smirnov, V. V., and Moore, G. W. K.: Spatial and temporal structure of atmospheric water vapor transport in the Mackenzie River basin, J. Climate, 12, 681-696, https://doi.org/10.1175/1520-0442(1999)012<0681:SATSOA>2.0.CO;2, 1999.

Sun, B., Zhu, Y., and Wang, H.: The recent interdecadal and interannual variation of water vapor transport over eastern China, Adv. Atmos. Sci., 28, 1039-1048, https://doi.org/10.1007/s00376-010-0093-1, 2011.

Tang, Y., Pang, H., Zhang, W., Li, Y., Wu, S., and Hou, S.: Effects of changes in moisture source and the upstream rainout on stable isotopes in precipitation–a case study in Nanjing, eastern China, Hydrol. Earth Syst. Sci., 19, 4293-4306, https://doi.org/10.5194/hess-19-4293-2015, 2015.

Vasil'chuk, Y. K.: New data on the tendency and causes of deuterium excess variations during one snowfall, Dokl. Earth Sci., 459, 1400-1403, https://doi.org/10.1134/S1028334X14110105, 2014.

Wei, Z., Lee, X., Liu, Z., Seeboonruang, U., Koike, M., and Yoshimura, K.: Influences of large-scale convection and moisture source on monthly precipitation isotope ratios observed in Thailand, Southeast Asia, Earth Planet. Sci. Lett., 488, 181-192, https://doi.org/10.1016/j.epsl.2018.02.015, 2018.

Wu, H., Fu, C., Zhang, C., Zhang, J., Wei, Z., and Zhang, X.: Temporal variations of stable isotopes in precipitation from Yungui Plateau: insights from moisture source and rainout effect, J. Hydrometeorol., 23, 39-51, https://doi.org/10.1175/JHM-D-21-0098.1, 2022.

Wu, H., Zhang, X., Xiaoyan, L., Li, G., and Huang, Y.: Seasonal variations of deuterium and oxygen-18 isotopes and their response to moisture source for precipitation events in the subtropical monsoon region, Hydrol. Process., 29, 90-102, https://doi.org/10.1002/hyp.10132, 2015. Nie, Y., & Sun, J. (2022). Moisture sources and transport for extreme precipitation over Henan in July 2021. Geophysical Research Letters, 49(4), 1-10.

Parding, K., Olseth, J. A., Liepert, B. G., & Dagestad, K. F. (2016). Influence of atmospheric circulation patterns on local cloud and solar variability in Bergen, Norway. Theoretical and Applied Climatology, 125, 625-639.

Pérez-Alarcón, A., Fernández-Alvarez, J. C., Sorí, R., Nieto, R., & Gimeno, L. (2023). Moisture source identification for precipitation associated with tropical cyclone development over the Indian Ocean: a Lagrangian approach. Climate Dynamics, 60(9), 2735-2758.

Pokam, W. M., Djiotang, L. A. T., & Mkankam, F. K. (2012). Atmospheric water vapor transport and recycling in Equatorial Central Africa through NCEP/NCAR reanalysis data. Climate Dynamics, 38, 1715-1729.

Pranindita, A., Wang-Erlandsson, L., Fetzer, I., & Teuling, A. J. (2022). Moisture recycling and the potential role of forests as moisture source during European heatwaves. Climate Dynamics, 58(1), 609-624.

Qian, L., Solomon, S. C., & Kane, T. J. (2009). Seasonal variation of thermospheric density and composition. Journal of Geophysical Research: Space Physics, 114(A1), 1-15.

Risi, C., Bony, S., Vimeux, F., Frankenberg, C., Noone, D., & Worden, J. (2010). Understanding the Sahelian water budget through the isotopic composition of water vapor and precipitation. Journal of Geophysical Research: Atmospheres, 115(D24), 1-23.

Risi, C., Noone, D., Frankenberg, C., & Worden, J. (2013). Role of continental recycling in intraseasonal variations of continental moisture as deduced from

model simulations and water vapor isotopic measurements. Water Resources Research, 49(7), 4136-4156.

Rozanski, K., Araguás-Araguás, L., & Gonfiantini, R. (1993). Isotopic patterns in modern global precipitation. Climate change in continental isotopic records, 78, 1-36.

Sengupta, S., & Sarkar, A. (2006). Stable isotope evidence of dual (Arabian Sea and Bay of Bengal) vapour sources in monsoonal precipitation over north India. Earth and Planetary Science Letters, 250(3-4), 511-521.

Shi, X., Risi, C., Li, L., Wang, X., Pu, T., Zhang, G., ... & Kong, Y. (2022). What controls the skill of general circulation models to simulate the seasonal cycle in water isotopic composition in the Tibetan Plateau region?. Journal of Geophysical Research: Atmospheres, 127(22), e2022JD037048.

Shi, Y., Jin, Z., Wu, A., Li, G., & Li, F. (2021). Stable isotopic characteristics of precipitation related to the environmental controlling factors in Ningbo, East China. Environmental Science and Pollution Research, 28, 10696-10706.

Smirnov, V. V., & Moore, G. W. K. (1999). Spatial and temporal structure of atmospheric water vapor transport in the Mackenzie River basin. Journal of Climate, 12(3), 681-696

Sun, B., Zhu, Y., & Wang, H. (2011). The recent interdecadal and interannual variation of water vapor transport over eastern China. Advances in Atmospheric Sciences, 28, 1039-1048.

Tang, Y., Pang, H., Zhang, W., Li, Y., Wu, S., & Hou, S. (2015). Effects of changes in moisture source and the upstream rainout on stable isotopes in precipitation - a case study in Nanjing, eastern China. Hydrology and Earth System Sciences, 19(10), 4293-4306.

Vasil'chuk, Y. K. (2014). New data on the tendency and causes of deuterium excess variations during one snowfall. Doklady Earth Sciences 459(1), 1400-1403.

Wei, Z., Lee, X., Liu, Z., Seeboonruang, U., Koike, M., & Yoshimura, K. (2018). Influences of large-scale convection and moisture source on monthly precipitation isotope ratios observed in Thailand, Southeast Asia. Earth and Planetary Science Letters, 488, 181-192.

Wu, H., Fu, C., Zhang, C., Zhang, J., Wei, Z., & Zhang, X. (2022). Temporal variations of stable isotopes in precipitation from Yungui Plateau: insights from moisture source and rainout effect. Journal of Hydrometeorology, 23(1), 39-51.

Wu, H., Zhang, X., Xiaoyan, L., Li, G., & Huang, Y. (2015). Seasonal variations of deuterium and oxygen-18 isotopes and their response to moisture source for precipitation events in the subtropical monsoon region. Hydrological Processes, 29(1), 90-102.

Xiao, Z., Zhang, X., Xiao, X., Chang, X., and He, X.: The Effect of Convective/Advective Precipitation Partitions on the Precipitation Isotopes in the Monsoon Regions of China: A Case Study of Changsha, J. Hydrometeorol., 23, 581-590, https://doi.org/10.1175/JHM-D-23-0084.1, 2024.

Xu, K., Zhong, L., Ma, Y., Zou, M., and Huang, Z.: A study on the water vapor transport trend and water vapor source of the Tibetan Plateau, Theor. Appl. Climatol., 140, 1031-1042, https://doi.org/10.1007/s00704-020-03142-2, 2020.

Xu, T., Sun, X., Hong, H., Wang, X., Cui, M., Lei, G., and Jiang, X.: Stable isotope ratios of typhoon rains in Fuzhou, Southeast China, during 2013–2017, J. Hydrol., 570, 445-453, https://doi.org/10.1016/j.jhydrol.2019.01.017, 2019.

Yoshimura, K., Kanamitsu, M., Noone, D., and Oki, T.: Historical isotope simulation using reanalysis atmospheric data, J. Geophys. Res.-Atmos., 113, D19101, https://doi.org/10.1029/2008JD010074, 2008.

Zhan, Z., Pang, H., Wu, S., Liu, Z., Zhang, W., Xu, T., and Hou, S.: Determining key upstream convection and rainout zones affecting $\delta^{18}O$ in water vapor and precipitation based on 10-year continuous observations in the East Asian Monsoon region, Earth Planet. Sci. Lett., 601, 117912, https://doi.org/10.1016/j.epsl.2022.117912, 2023.

Zhang, H., Cheng, H., Cai, Y., Spötl, C., Sinha, A., Kathayat, G., and Li, H.: Effect of precipitation seasonality on annual oxygen isotopic composition in the area of spring persistent rain in southeastern China and its paleoclimatic implication, Clim. Past, 16, 211-225, https://doi.org/10.5194/cp-16-211-2020, 2020.

Zhang, X., Guan, H., Zhang, X., He, X., Zhang, W., Wang, X., and Yao, T.: Comparisons and assessment on stable isotopic effects in precipitation simulated by different models (in Chinese with English abstract), Quat. Sci., 36, 1343-1357, https://doi.org/10.11928/j.issn.1001-7410.2016.06.01, 2016.

Zhang, X., Sun, Z., Guan, H., Zhang, X., Wu, H., and Huang, Y.: GCM simulations of stable isotopes in the water cycle in comparison with GNIP observations over East Asia, Acta Meteorol. Sinica, 26, 420-437, https://doi.org/10.1007/s13351-012-0403-x, 2012.

Zhou, H., Zhang, X., Yao, T., Hua, M., Wang, X., Rao, Z., and He, X.: Variation of $\delta^{18}O$ in precipitation and its response to upstream atmospheric convection and rainout: A case study of Changsha station, south-central China, Sci. Total Environ., 659, 1199-1208, https://doi.org/10.1016/j.scitotenv.2018.12.396, 2019. Xiao, Z., Zhang, X., Xiao, X., Chang, X., & He, X. (2024). The Effect of Convective/Advective Precipitation Partitions on the Precipitation Isotopes in the Monsoon Regions of China: A Case Study of Changsha. Journal of Hydrometeorology, 23(84), 581-590.

Xu, K., Zhong, L., Ma, Y., Zou, M., & Huang, Z. (2020). A study on the water vapor transport trend and water vapor source of the Tibetan Plateau. Theoretical and Applied Climatology, 140, 1031-1042.

Xu, T., Sun, X., Hong, H., Wang, X., Cui, M., Lei, G., ... & Jiang, X. (2019). Stable isotope ratios of typhoon rains in Fuzhou, Southeast China, during 2013 2017. Journal of Hydrology, 570, 445-453.

Yoshimura, K., Kanamitsu, M., Noone, D., & Oki, T. (2008). Historical isotope simulation using reanalysis atmospheric data. Journal of Geophysical Research: Atmospheres, 113(D19), 1-15.

Zhan, Z., Pang, H., Wu, S., Liu, Z., Zhang, W., Xu, T., ... & Hou, S. (2023). Determining key upstream convection and rainout zones affecting $\delta^{18}O$ in water vapor and precipitation based on 10-year continuous observations in the East Asian Monsoon region. Earth and Planetary Science Letters, 601, 117912.

Zhang, H., Cheng, H., Cai, Y., Spötl, C., Sinha, A., Kathayat, G., & Li, H. (2020). Effect of precipitation seasonality on annual oxygen isotopic composition in the area of spring persistent rain in southeastern China and its paleoclimatic implication. Climate of the Past, 16(1), 211-225.

Zhang, X., Guan, H., Zhang, X., He, X., Zhang, W., Wang, X., & Yao, T. (2016). Comparisons and assessment on stable isotopic effects in precipitation simulated by different models. Quaternary Sciences, 36(6), 1343-1357.

Zhang, X., Sun, Z., Guan, H., Zhang, X., Wu, H., & Huang, Y. (2012). GCM simulations of stable isotopes in the water cycle in comparison with GNIP observations over East Asia. Acta Meteorologica Sinica, 26(4), 420-437.

Zhou, H., Zhang, X., Yao, T., Hua, M., Wang, X., Rao, Z., & He, X. (2019). Variation of $\delta^{18}O$ in precipitation and its response to upstream atmospheric convection and rainout: A case study of Changsha station, south-central China. Science of the total environment, 659, 1199-1208. Zhou, H., Zhang, X., Yao, T., Luo, Z., Hua, M., and Sun, H.: $\delta^{18}O$ in precipitation and water vapor transfer in the summer half year in China (in Chinese with English abstract), Quat. Sci., 38, 314-326, https://doi.org/10.11928/j.issn.1001-7410.2018.02.04, 2018.

1414   Zhou, S. Z. (1997). Meteorology and Climatology. Higher Education Press, Beijing,

1415   118-222.Zhou, S. Z. (Eds.): Meteorology and Climatology (in Chinese), Higher

1416   Education Press, Beijing, China, 118-222 pp., ISBN 9787040060164, 1997.

1417